DESY 95–048
MPI/PhT/95–20
hep-ph/9503207
March 1995

ISSN 0418-9833

Pion and Kaon Production in e^+e^- and ep Collisions at Next-to-Leading Order

J. Binnewies[1], B.A. Kniehl[2], and G. Kramer[1]
[1] II. Institut für Theoretische Physik*, Universität Hamburg
Luruper Chaussee 149, 22761 Hamburg, Germany
[2] Max-Planck-Institut für Physik, Werner-Heisenberg-Institut
Föhringer Ring 6, 80805 Munich, Germany

Abstract

We present new sets of fragmentation functions for charged pions and kaons, both at leading and next-to-leading order. They are fitted to data on inclusive charged-hadron production in e^+e^- annihilation taken by TPC at PEP ($\sqrt{s} = 29$ GeV) and to similar data by ALEPH at LEP, who discriminated between events with charm, bottom, and light-flavour fragmentation in their charged-hadron sample. In contrast to our previous analysis, where we only distinguished between valence-quark, sea-quark, and gluon fragmentation, we are now able to treat all partons independently and to properly incorporate the charm and bottom thresholds. Due to the sizeable energy gap between PEP and LEP, we are sensitive to the scaling violation in the fragmentation process, which allows us to extract a value for the asymptotic scale parameter of QCD, Λ. Recent data on inclusive charged-hadron production in tagged three-jet events by OPAL and similar data for longitudinal electron polarization by ALEPH allow us to pin down the gluon fragmentation functions. Our new fragmentation functions lead to an excellent description of a multitude of other e^+e^- data on inclusive charged-hadron production, ranging from $\sqrt{s} = 5.2$ GeV to LEP energy. In addition, they agree nicely with the transverse-momentum spectra of single charged hadrons measured by H1 and ZEUS in photoproduction at the ep collider HERA, which represents a nontrivial check of the factorization theorem of the QCD-improved parton model. In this comparison, we also find first evidence for the interplay between the direct- and resolved-photon mechanisms and for the existence of a gluon density inside the photon.

*Supported by Bundesministerium für Forschung und Technologie, Bonn, Germany, under Contract 05 6 HH 93P (5), and by EEC Program *Human Capital and Mobility* through Network *Physics at High Energy Colliders* under Contract CHRX-CT93-0357 (DG12 COMA).

1 Introduction

The advent of precise data on inclusive hadron production at $p\bar{p}$, ep, and e^+e^- colliders offers the challenging opportunity to test quantitatively the QCD-improved parton model. The inclusive cross section is expressed as a convolution of the parton density functions (PDF), the partonic cross sections, and the fragmentation functions (FF) of the quarks and gluons into the outgoing hadrons. The factorization theorem ensures that the PDF and FF are universal and that only the hard-scattering partonic cross sections change when different processes are considered. While there exist highly sophisticated sets of the PDF for the incoming protons and photons, which are needed for the analysis of inclusive particle production in $p\bar{p}$ and ep reactions, the status of the quark and gluon FF is much less advanced. The most direct way to obtain information on the FF is to analyse the energy spectrum of the hadrons into which the jets produced by e^+e^- annihilation fragment.

Recently, we performed such an analysis to extract FF for charged pions and kaons at leading order (LO) and next-to-leading order (NLO) in QCD [1]. These FF were generated through fits to e^+e^--annihilation data taken at centre-of-mass (CM) energy $\sqrt{s} = 29$ GeV by the TPC Collaboration at SLAC [2]. About one year ago, these were the most precise data for charged-pion and -kaon production. Our FF also led to rather satisfactory descriptions of other e^+e^- data on charged-particle production at lower (DORIS [3,4]), similar (PEP [5]), and higher energies (PETRA [6,7], TRISTAN [8], and LEP [9]).

These new parameterizations—in particular, the NLO sets—were tested against data on single-charged-hadron production obtained by the H1 Collaboration in ep-scattering experiments at HERA [10] in Refs. [10,11] and against similar data obtained in various $p\bar{p}$ experiments in Ref. [12]. The agreement between experimental data and theory turned out to be very satisfactory. This motivates us to further improve the FF, especially since detailed high-statistics data on charged-hadron production at LEP have become available [13,14,15,16]. For our extended analysis, we shall employ very accurate data from the ALEPH Collaboration at LEP, who partly discriminated between pions and kaons [14]. In the data sample without discrimination of the hadron species, they distinguished between three cases, namely fragmentation of (i) u, d, and s quarks, (ii) b quarks only, and (iii) all five quark flavours (u, d, s, c, and b). In particular, the latter data on the fragmentation of specific quark flavours enables us to remove a theoretical assumption which we had to make in our earlier work [1], namely that the s, c, and b (d, c, and b) quarks fragment into charged pions (kaons) in the same way. As is well known, b quarks are produced considerably more copiously at the Z resonance than at lower CM energies. Therefore, ALEPH was able to separate the fragmentation of b quarks into charged hadrons from the fragmentation of all other quarks. On the basis of these new ALEPH data on charged-hadron production, Cowan [13] has performed a similar analysis using the Altarelli-Parisi (AP) equations [17] for the Q^2 evolution and incorporating data from other experiments at lower energy. The scope of his analysis is quite different from ours. He concentrates on charged-hadron data and is chiefly interested in establishing the scaling violation so as to determine $\alpha_s(M_Z^2)$. Another significant difference is that he uses a rather high starting

scale, $Q_0 = 22$ GeV, which lies well above the scale characteristic for our ep studies. Similarly to the case of the PDF, the method of choice for our purposes it to use simple parameterizations at the low threshold scales.

A problem that requires special attention is related to the gluon fragmentation into charged hadrons. Although the gluon does not couple directly to the electroweak currents, it contributes in higher orders and mixes with the quarks through the Q^2 evolution. This renders it very difficult to pin down the gluon FF by using just the energy spectrum of hadrons produced by e^+e^- annihilation. However, the gluon fragmentation can be probed in e^+e^- annihilation by exploiting tagged three-jet events or longitudinal polarization. As in our earlier work [1], we use the information on tagged three-jet events made available by the OPAL Collaboration [15] to test our gluon FF. Recently, in Ref. [12], it was shown that a sufficiently sizeable gluon FF into charged hadrons is essential to reach good agreement with the data of single-charged hadron production in $p\bar{p}$ processes. Since gluon production is also significant in ep collisions at HERA, we should be able to further test the strength of the gluon FF extracted from e^+e^- data by making comparisons with data on inclusive photoproduction of charged hadrons recently collected by the H1 [10] and ZEUS Collaborations [18].

It is the purpose of this work to make use of the recent data by ALEPH [13,14] in addition to the data by TPC [2] and OPAL [15] to construct new sets of LO and NLO FF without imposing identities between the FF of different flavours. (We shall still identify the FF of u and d quarks into charged pions and those of u and s quarks into charged kaons.) The new FF sets will be tested against additional e^+e^- data from LEP and e^+e^- colliders with lower CM energies. In addition, we shall study single-charged hadron production in ep collisions under HERA conditions in order to check the consistency of our FF with the new H1 [10] and ZEUS data [18], in particular with respect to the issue of the gluon FF.

This work is organized as follows. In Section 2, we shall introduce the formalism needed to extract the FF from e^+e^- data on inclusive single-hadron production at NLO. In Section 3, we shall present the formulae that describe inclusive single-hadron production in ep collisions with almost real photons. Section 4 will deal with the actual analysis and the discussion of our results. In Section 5, we shall check our results against e^+e^- data which we did not use in our fits and against the recent H1 and ZEUS data. Our conclusions will be summarized in Section 6. As in our earlier work [1], we shall list, in the Appendix, simple parameterizations of our FF sets.

2 Formalism for e^+e^- reactions

The inclusive production of a hadron h by e^+e^- annihilation,

$$e^+e^- \to (\gamma, Z) \to h + X, \tag{1}$$

is completely characterized by three observables. These are the energy fraction of the outgoing hadron $x = 2E_h/\sqrt{s}$, its angle with the beam axis θ and the total energy of the

system $\sqrt{s}$. The cross section of process (1) exhibits the angular structure

$$\frac{d^2\sigma(e^+e^- \to h + X)}{dx\, d\cos\theta} = \frac{3}{8}(1+\cos^2\theta)\frac{d\sigma^T}{dx} + \frac{3}{4}\sin^2\theta\frac{d\sigma^L}{dx} + \frac{3}{4}\cos\theta\frac{d\sigma^A}{dx}, \tag{2}$$

where the superscripts T and L denote the contributions due to transverse and longitudinal polarizations, respectively, and the asymmetric term, labelled A, accounts for the interference of the photon with the Z boson. Usually, experiments do not determine θ distributions. Thus we shall integrate over θ. This eliminates the asymmetric term in Eq. (2).

The partonic subprocesses may be exactly treated in perturbative QCD. However, this is not yet possible for the process of hadronization. As explained in the Introduction, the latter is described in terms of phenomenological FF, which must be extracted from experiment. In the language of the QCD-improved parton model, the x distribution of process (1) emerges from the x distribution, $(d\sigma_a/dx)(x,\mu^2,Q^2)$, of $e^+e^- \to a+X$ through convolution with $D_a^h(x,Q^2)$,

$$\frac{1}{\sigma_{tot}}\frac{d\sigma(e^+e^- \to h + X)}{dx} = \sum_a \int_x^1 \frac{dz}{z}\, D_a^h(z,M_f^2)\, \frac{1}{\sigma_{tot}}\frac{d\sigma_a}{dy}\left(\frac{x}{z},\mu^2,M_f^2\right). \tag{3}$$

Here, the sum extents over all active partons ($a = u,d,s,c,b,g$), μ is the renormalization scale of the partonic subprocess, and M_f is the so-called fragmentation scale. At NLO, M_f defines the point where the divergence associated with collinear radiation off parton a is to be subtracted. Throughout this paper, we neglect finite-quark-mass effects in the matrix elements. In order to be able to compare our calculations with experimental data, we normalize the cross section to

$$\sigma_{tot} = N_c \sum_{i=1}^{N_f} e_{q_i}^2 \sigma_0, \tag{4}$$

where $\sigma_0 = (4\pi\alpha^2/3s)$ is the total cross section of $e^+e^- \to \mu^+\mu^-$ for massless leptons, $N_c = 3$, e_{q_i} is the electroweak charge of quark q_i in units of the positron charge, and N_f is the number of active flavors. In Eq. (4), we take into account the running of the fine-structure constant, α, and the enhancement of the contributions due to down-type quarks at the Z pole. Since the absolute normalization is determined experimentally only to the 4% level, we neglect corrections to $\sigma_{\rm tot}$ in higher orders of α_s.

To NLO in the $\overline{\rm MS}$ scheme, the cross sections of the relevant subprocesses are given by

$$\begin{aligned}
\frac{1}{\sigma_{tot}}\frac{d\sigma_{q_i}}{dy}(y,\mu^2,M_f^2) &= e_{q_i}^2 N_c \frac{\sigma_0}{\sigma_{tot}}\left\{\delta(1-y) + \frac{\alpha_s(\mu^2)}{2\pi}\left[P_{qq}^{(0,T)}(y)\ln\frac{s}{M_f^2} + K_q^T(y) + K_q^L(y)\right]\right\},\\
\frac{1}{\sigma_{tot}}\frac{d\sigma_g}{dy}(y,\mu^2,M_f^2) &= 2\frac{\alpha_s(\mu^2)}{2\pi}\left[P_{qg}^{(0,T)}(y)\ln\frac{s}{M_f^2} + K_g^T(y) + K_g^L(y)\right].
\end{aligned} \tag{5}$$

$P_{ab}^{(0,T)}(y)$ is the LO term of the transverse $a \to b$ splitting function,

$$P_{ab}^{T}(y,\alpha_s(Q^2)) = P_{ab}^{(0,T)}(y) + \frac{\alpha_s(Q^2)}{2\pi} P_{ab}^{(1,T)}(y) + \cdots . \tag{6}$$

The K functions have been presented in Ref. [19]. The NLO formula of $\alpha_s(\mu^2)$ may be found, *e.g.*, in Ref. [20]. The scales μ and M_f are usually identified with the only intrinsic energy scale, $\sqrt{s}$. For this choice of scales, the terms in Eq. (5) involving $\ln(s/M_f^2)$ are suppressed, so that the NLO corrections are expressed just in terms of the K functions. At LO, only the transversely polarized photon contributes to the cross section. The longitudinal cross sections of the subprocesses are thus given by

$$\begin{aligned}
\frac{1}{\sigma_{tot}} \frac{d\sigma_{q_i}^L}{dy}(y,\mu^2,M_f^2) &= \frac{\alpha_s(\mu^2)}{2\pi}\, C_F\, e_{q_i}^2 N_c \frac{\sigma_0}{\sigma_{tot}}, \\
\frac{1}{\sigma_{tot}} \frac{d\sigma_{g}^L}{dy}(y,\mu^2,M_f^2) &= \frac{\alpha_s(\mu^2)}{2\pi}\, C_F\, \frac{4(1-y)}{y}.
\end{aligned} \tag{7}$$

Having defined the partonic subprocesses, we now turn to the FF. Their x distributions are not yet calculable in the framework of perturbative QCD. However, once we know them at some scale Q_0^2, the Q^2 evolution is determined by the AP equations [17]. Our task is thus to construct a model for the x distributions at a starting scale Q_0^2, which, after evolution, fits the data at scale Q^2. The AP equations read

$$\frac{d}{d\ln Q^2} D_a^h(x,Q^2) = \frac{\alpha_s(Q^2)}{2\pi} \sum_b \int_x^1 \frac{dy}{y} P_{ba}^T(y,\alpha_s(Q^2)) D_b^h\left(\frac{x}{y},Q^2\right). \tag{8}$$

That is, we have to solve a system of integro-differential equations. This may be achieved with the help of the Mellin-transform technique [21]. The essential property of this transformation is that it renders convolutions to products. In fact, denoting the moments of P_{ab}^T and D_a^h by A_{ab} and M_a, respectively, we have

$$\begin{aligned}
\frac{d}{d\ln Q^2} M_i^+(n,Q^2) &= \frac{\alpha_s(Q^2)}{2\pi} A_{NS}(n,\alpha_s(Q^2)) M_i^-(n,Q^2), \\
\frac{d}{d\ln Q^2} M_\Sigma(n,Q^2) &= \frac{\alpha_s(Q^2)}{2\pi} \left[A_{qq}(n,\alpha_s(Q^2)) M_\Sigma(n,Q^2) + A_{gq}(n,\alpha_s(Q^2)) M_G(n,Q^2)\right], \\
\frac{d}{d\ln Q^2} M_G(n,Q^2) &= \frac{\alpha_s(Q^2)}{2\pi} \left[A_{qg}(n,\alpha_s(Q^2)) M_\Sigma(n,Q^2) + A_{gg}(n,\alpha_s(Q^2)) M_G(n,Q^2)\right],
\end{aligned} \tag{9}$$

where A_{NS} refers to the usual non-singlet combination of quark and antiquark splitting functions [21], the LO expressions for A_{ab} may be found in Refs. [21,22] and the NLO ones in Ref. [23], and

$$\begin{aligned}
M_i^+(n,Q^2) &= \frac{1}{2}\left[M_{q_i}(n,Q^2) + M_{\bar{q}_i}(n,Q^2)\right] - \frac{1}{2N_f} M_\Sigma(n,Q^2), \\
M_\Sigma(n,Q^2) &= \sum_{i=1}^{N_f} \left[M_{q_i}(n,Q^2) + M_{\bar{q}_i}(n,Q^2)\right], \\
M_G(n,Q^2) &= M_g(n,Q^2).
\end{aligned} \tag{10}$$

We do not include combinations $M_i^- = M_{q_i} - M_{\bar{q}_i}$, which are asymmetric under baryon-number symmetry, since we do not distinguish between quarks and antiquarks. Note that the non-singlet terms, M_i^+, decouple from the gluon. The solutions of Eq. (9) factorize,

$$M(n, Q_2^2) = E(Q_1^2, Q_2^2, N_f)\, M(n, Q_1^2). \tag{11}$$

The relevant evolution operators, $E(Q_1^2, Q_2^2)$, have been calculated in Ref. [21]. For instance, in the non-singlet case, the NLO operator reads

$$E_{NS}^{(0)}(Q_1^2, Q_2^2, N_f) = \left[\frac{\alpha_s(Q_1^2)}{\alpha_s(Q_2^2)}\right]^{\frac{2}{\beta_0}A_{NS}^{(0)}} \left[1 + \frac{\alpha_s(Q_2^2) - \alpha_s(Q_1^2)}{2\pi}\left(\frac{\beta_1}{\beta_0^2}A_{NS}^{(0)} - \frac{2}{\beta_0}A_{NS}^{(1)}\right)\right], \tag{12}$$

where $\beta_0 = (33 - 2N_f)/3$ and $\beta_1 = (153 - 19N_f)/3$. The corresponding equation for the coupled system exhibits a similar structure and is omitted here for ease of presentation. The subtraction in Eq. (12) has the effect that, at $Q^2 = Q_0^2$, the FF are equal to the ansatz also at NLO. In this respect, we differ from the approach of Ref. [1]. We evolve the FF in three steps. We start with three quark flavours at the scale Q_0 and evolve up to the charm threshold using the evolution operators $E(Q_0^2, 4m_c^2, 3)$. There the charm FF is added to the set of FF, which, in the second step, are evolved to the bottom threshold employing $E(4m_c^2, 4m_b^2, 4)$. In the final step, the FF of all five quark flavours are evolved to the considered CM energy Q^2 with the help of $E(4m_b^2, Q^2, 5)$.

Strictly speaking, our QCD formalism is appropriate only for the strongly produced pions and kaons. However, a minor fraction of the observed events are due to pions and kaons that are produced through weak decays of primary D and B mesons. In this case, it is unclear whether the usual Q^2 evolution may be applied. In our analysis, we assumed that this may be done. A more careful study would require that the experiments discriminate strongly and weakly produced pions and kaons, which was not the case for the data used here.

3 Formalism for ep reactions

In this section, we shall outline the formalism pertinent to inclusive photoproduction of hadrons with ep colliders, and in particular with HERA. According to present HERA conditions, $E_e = 26.7$ GeV electrons collide with $E_p = 820$ GeV protons in the laboratory frame, so that $\sqrt{s} = 296$ GeV is available in the CM frame. Among the experimentalists it has become customary to take the rapidity, $y_{\rm lab}$, of hadrons travelling in the proton direction to be positive. The CM rapidity, $y_{\rm CM}$, is related to $y_{\rm lab}$ by

$$y_{\rm CM} = y_{\rm lab} - \frac{1}{2}\ln\frac{E_p}{E_e}. \tag{13}$$

In photoproduction, the electron beam acts like a source of quasi-real photons, so that HERA is effectively operated as a γp collider. The appropriate events may be discriminated from deep-inelastic-scattering events by electron tagging or anti-tagging. The

photon flux is well approximated by the Weizsäcker-Williams formula [24],

$$f_{\gamma/e}(z) = \frac{\alpha}{2\pi}\left[\frac{1+(1-z)^2}{z}\ln\frac{Q^2_{\max}}{Q^2_{\min}} + 2m_e^2 z\left(\frac{1}{Q^2_{\max}} - \frac{1}{Q^2_{\min}}\right)\right], \tag{14}$$

where $z = E_\gamma/E_e$, $Q^2_{\min} = m_e^2 z^2/(1-z)$, and $Q^2_{\max} = 0.01$ GeV^2 (0.02 GeV^2) for tagged events at H1 (ZEUS). The cross section of $ep \to h + X$ emerges from the one of $\gamma p \to h + X$ by convolution with $f_{\gamma/e}(z)$. By kinematics, $z_{\min} \le z \le 1$, where $z_{\min} = p_T \exp(-y_{\rm CM})/[\sqrt{s} - p_T \exp(y_{\rm CM})]$. In our analysis, we shall impose $0.3 < z < 0.7$ and $0.318 < z < 0.431$ to be in conformity with the H1 and ZEUS event-selection criteria, respectively.

It is well known that $\gamma p \to h + X$ proceeds via two distinct mechanisms. The photon can interact either directly with the partons originating from the proton (direct photoproduction) or via its quark and gluon content (resolved photoproduction). Both contributions are formally of the same order in the perturbative expansion. Leaving aside the proton PDF, $G_b^p(x, M_p^2)$, and the FF, $D_c^h(x, M_h^2)$, which represent common factors, the LO cross sections are of $O(\alpha\alpha_s)$ in both cases. In the case of the resolved mechanism, this may be understood by observing that the $ab \to cd$ cross sections, which are of $O(\alpha_s^2)$, get dressed by photon PDF, $G_a^\gamma(x, M_\gamma^2)$, whose leading terms are of the form $\alpha \ln(M_\gamma^2/\Lambda^2) \propto \alpha/\alpha_s$, with Λ being the asymptotic scale parameter of QCD. Here, a, b, c, d denote quarks and gluons. In fact, the two mechanisms also compete with each other numerically. Resolved photoproduction dominates at small p_T and positive $y_{\rm lab}$, while direct photoproduction wins out at large p_T and negative $y_{\rm lab}$.

The LO calculation suffers from significant theoretical uncertainties connected with the freedom in the choice of the renormalization scale, μ, of $\alpha_s(\mu^2)$ and the factorization scales, M_γ, M_p, M_h.[1] In order to obtain reliable predictions, it is indispensable to proceed to NLO. We shall first consider resolved photoproduction, which is more involved. Starting out from the well-known LO cross section of $\gamma p \to h + X$, one needs to include the NLO corrections, $K_{ab\to c}$, to the hard-scattering cross sections, to substitute the two-loop formula for α_s, and to endow G_a^γ, G_b^p, and D_c^h with NLO evolution. This leads to

$$E_h \frac{d^3\sigma(\gamma p \to h + X)}{d^3 p_h} = \sum_{a,b,c} \int dx_\gamma dx_p \frac{dx_h}{x_h^2}\, G_a^\gamma(x_\gamma, M_\gamma^2) G_b^p(x_p, M_p^2) D_c^h(x_h, M_h^2)$$
$$\times \frac{1}{\pi\hat{s}}\left[\frac{1}{v}\frac{d\sigma^0_{ab\to c}}{dv}(\hat{s}, v; \mu^2)\delta(1-w) + \frac{\alpha_s(\mu^2)}{2\pi} K_{ab\to c}(\hat{s}, v, w; \mu^2, M_\gamma^2, M_p^2, M_h^2)\right], \tag{15}$$

where $d\sigma^0_{ab\to c}/dv$ are the LO hard-scattering cross sections, $v = 1 + \hat{t}/\hat{s}$, and $w = -\hat{u}/(\hat{s} + \hat{t})$, with $\hat{s} = (p_a + p_b)^2$, $\hat{t} = (p_a - p_c)^2$, and $\hat{u} = (p_b - p_c)^2$ being the Mandelstam variables at the parton level. The parton momenta are related to the photon, proton, and hadron momenta by $p_a = x_\gamma p_\gamma$, $p_b = x_p p_p$, and $p_c = p_h/x_h$. The indices a, b, c run over the gluon and N_f flavours of quarks and antiquarks. In this paper, we shall take $N_f = 5$. The

[1] The LO cross section of direct photoproduction does not depend on M_γ.

$K_{ab\to c}$ functions may be found in Ref. [25] for $M_\gamma = M_p$. This restriction was relaxed in Ref. [26].

The NLO cross section of direct photoproduction emerges from Eq. (15) by substituting $G_a^\gamma(x_\gamma, M_\gamma^2) = \delta(1-x_\gamma)$, replacing $d\sigma_{ab\to c}/dv$ and $K_{ab\to c}$ by $d\sigma_{\gamma b\to c}/dv$ and $K_{\gamma b\to c}$, respectively, and omitting the sum over a. The $K_{\gamma b\to c}$ functions were first derived in Ref. [27] setting $M_\gamma = M_p = M_h$ and taking the spin-average for incoming photons and gluons to be 1/2. In Ref. [26], the scales were disentangled and the spin-average convention was converted to the $\overline{\rm MS}$ scheme, *i.e.*, to be $1/(n-2)$, with n being the dimensionality of space-time. Analytic expressions for the $K_{\gamma b\to c}$ functions are listed in Ref. [28]. Quantitative studies of inclusive photoproduction of hadrons at HERA via the direct- and resolved-photon mechanisms in NLO may be found in Refs. [26,28,29].

4 Results

In general, data of inclusive hadron production at e^+e^- colliders are most suitable for the extraction of the FF; in the case of fixed-target, collider, and ep data, the information on the FF is obscured by theoretical uncertainties arising from the PDF and the choice of factorization scales connected with the initial state. For our analysis, we select the data on charged-pion and -kaon production taken at energy $\sqrt{s} = 29$ GeV by the TCP Collaboration at SLAC [2] and those collected at $\sqrt{s} = M_Z$ by the ALEPH Collaboration at LEP [14]. In order to constrain the FF of the different quark flavours, we employ the ALEPH data [13] on charged-hadron production for the three cases: (1) sum over all quark flavours (u, d, s, c, b); (2) sum over u, d, s quarks; and (3) b quark. These data combine small statistical errors with fine binning in x and are thus more constraining than data collected by other e^+e^- experiments in the energy range from 5.2 to 55 GeV. For this reason, our approach is to fit exclusively to TPC and ALEPH data and to use the other data for cross checks. To control the gluon FF, we exploit, as in our previous work [1], the information on the tagged three-jet events by OPAL [15] presented by Nason and Webber [15], who applied small corrections to the original data. However, these data comprise just five points and are not very constraining. For the fitting procedure, we use the x bins in the interval between $x_{\rm min} = \max(0.1, 2\ {\rm GeV}/\sqrt{s})$ and 0.8 and integrate the theoretical functions over the bin widths as in the experimental data. The restriction at small x is necessary to exclude events in the non-perturbative region, where mass effects are important and our formalism is bound to fail. We parameterize the x dependence of the FF at Q_0^2 as

$$D_a^h(x, Q_0^2) = N x^\alpha (1-x)^\beta. \tag{16}$$

In contrast to our previous work [1], we now only impose the conditions $D_d^{\pi^+ + \pi^-} = D_u^{\pi^+ + \pi^-}$ and $D_s^{K^+ + K^-} = D_u^{K^+ + K^-}$. For all the other FF, including those of the gluon, we keep N, α, and β as independent fit parameters. This means that, together with Λ, which we also keep as a free parameter, we have a total of 31 independent fit parameters.

The quality of the fit is measured in terms of the average $\chi^2_{\rm d.o.f.}$ for all selected data points. Our technical procedure is as follows. We consider Eq. (3) at $\mu = M_f = \sqrt{s} =$

29 GeV and M_Z as a function of the 31 parameters that determine the x dependence of the FF at the respective values of Q_0, which we take to be $Q_0 = \sqrt{2}$ GeV for u, d, s, $Q_0 = m(\eta_c) = 2.9788$ GeV [20] for c, and $Q_0 = m(\Upsilon) = 9.46037$ GeV [20] for b. Using a multidimensional minimization algorithm [30], we search this 31-dimensional parameter space for the point at which the deviation of the theoretical prediction from the data becomes minimal. When we fit to charged-hadron data, we must include the contribution due to protons and antiprotons. To this end, we introduce a function, $f(x)$, which parameterizes the ratio of the cross sections of $p+\bar{p}$ and $\pi^+ + \pi^-$ production as measured by ALEPH [14],

$$f(x) = 0.195 - 1.35\,(x - 0.35)^2. \tag{17}$$

Thus, the charged-particle production cross section is given by

$$\frac{d\sigma^{h^+ + h^-}}{dx} = [1 + f(x)]\frac{d\sigma^{\pi^+ + \pi^-}}{dx} + \frac{d\sigma^{K^+ + K^-}}{dx}. \tag{18}$$

To test the perturbative stability, we perform fits in LO and NLO, although we are primarily interested in the NLO results.

Our results are listed below. For the average of charged pions, we obtain

$$\begin{aligned}
D_u^{(\pi,LO)}(x,Q_0^2) &= D_d^{(\pi,LO)}(x,Q_0^2) = 1.09\,x^{-0.842}\,(1-x)^{1.43},\\
D_s^{(\pi,LO)}(x,Q_0^2) &= 3.47\,x^{-1.037}\,(1-x)^{3.88},\\
D_c^{(\pi,LO)}(x,Q_0^2) &= 4.52\,x^{-0.898}\,(1-x)^{4.69},\\
D_b^{(\pi,LO)}(x,Q_0^2) &= 3.62\,x^{-1.128}\,(1-x)^{7.12},\\
D_g^{(\pi,LO)}(x,Q_0^2) &= 6.20\,x^{-0.351}\,(1-x)^{3.00}
\end{aligned} \tag{19}$$

in LO and

$$\begin{aligned}
D_u^{(\pi,NLO)}(x,Q_0^2) &= D_d^{(\pi,NLO)}(x,Q_0^2) = 1.16\,x^{-0.762}\,(1-x)^{1.47},\\
D_s^{(\pi,NLO)}(x,Q_0^2) &= 3.96\,x^{-0.825}\,(1-x)^{4.38},\\
D_c^{(\pi,NLO)}(x,Q_0^2) &= 3.69\,x^{-0.873}\,(1-x)^{5.06},\\
D_b^{(\pi,NLO)}(x,Q_0^2) &= 4.00\,x^{-1.037}\,(1-x)^{7.75},\\
D_g^{(\pi,NLO)}(x,Q_0^2) &= 5.11\,x^{-0.287}\,(1-x)^{2.61}
\end{aligned} \tag{20}$$

in NLO. In the case of kaons, we find

$$\begin{aligned}
D_u^{(K,LO)}(x,Q_0^2) &= D_s^{(K,LO)}(x,Q_0^2) = 0.38\,x^{-1.234}\,(1-x)^{1.04},\\
D_d^{(K,LO)}(x,Q_0^2) &= 1.11\,x^{-0.942}\,(1-x)^{2.81},\\
D_c^{(K,LO)}(x,Q_0^2) &= 0.55\,x^{-0.764}\,(1-x)^{2.69},\\
D_b^{(K,LO)}(x,Q_0^2) &= 0.72\,x^{-0.792}\,(1-x)^{2.81},\\
D_g^{(K,LO)}(x,Q_0^2) &= 0.43\,x^{-0.374}\,(1-x)^{2.69}
\end{aligned} \tag{21}$$

TABLE I. CM energies, types of data, numbers of data points used, and $\chi^2_{\rm d.o.f.}$ values obtained at NLO and LO for the various data samples discussed in the text. The data used in the fits are marked by an asterisk.

$\sqrt{s}$ [GeV]	Data type		Ref.	No. of points	$\chi^2_{\rm d.o.f.}$ in NLO	$\chi^2_{\rm d.o.f.}$ in LO
91.2	σ^h (all flavours)	*	[13]	23	0.84	0.85
	σ^h (u,d,s)	*	[13]	23	1.13	1.41
	σ^h (b)	*	[13]	23	1.06	0.84
	σ^π	*	[14]	13	1.19	1.30
	σ^K	*	[14]	13	1.10	1.57
	D_g^h	*	[15]	5	7.05	6.22
	σ^h (longitudinal)		[13]	10	8.65	–
	σ^h (all flavours)		[9]	22	0.95	0.82
55.2	σ^h		[8]	7	1.18	1.23
43.7	σ^π		[7]	3	0.94	0.92
35.0	σ^h		[6]	22	0.64	1.24
34.0	σ^π		[7]	6	0.63	0.54
	σ^K		[7]	2	0.66	0.99
29.0	σ^h		[5]	14	1.55	2.13
	σ^π	*	[2]	18	1.30	1.49
	σ^K	*	[2]	18	0.88	0.75
9.98	σ^π		[4]	19	1.56	1.88
	σ^K		[4]	14	1.00	1.35
5.20	σ^π		[3]	5	0.93	0.45
	σ^K		[3]	3	1.49	2.31

in LO and

$$
\begin{aligned}
D_u^{(K,NLO)}(x,Q_0^2) &= D_s^{(K,NLO)}(x,Q_0^2) = 0.30\,x^{-0.978}\,(1-x)^{1.01},\\
D_d^{(K,NLO)}(x,Q_0^2) &= 1.05\,x^{-0.804}\,(1-x)^{2.54},\\
D_c^{(K,NLO)}(x,Q_0^2) &= 0.68\,x^{-0.753}\,(1-x)^{2.59},\\
D_b^{(K,NLO)}(x,Q_0^2) &= 0.58\,x^{-0.843}\,(1-x)^{2.88},\\
D_g^{(K,NLO)}(x,Q_0^2) &= 0.33\,x^{-0.351}\,(1-x)^{0.65}
\end{aligned}
\tag{22}
$$

in NLO. Here, it is understood that the Q_0^2 values refer to the individual starting points given above. The $\chi^2_{\rm d.o.f.}$ values achieved for the different data sets may be seen from Table I.

For the reader's convenience, we list simple parameterizations of the x and Q^2 dependences of these sets in the Appendix. We believe that such parameterizations are indispensable for practical purposes, especially at NLO. However, we should caution the reader that these parameterizations describe the evolution of the FF only approximately. Deviations in excess of 10% may occur for $x < 0.1$, in particular for the gluon. While this kind of accuracy is fully satisfactory for most applications, it is insufficient for the

comparison with the high-statistics data collected at LEP. We wish to point out that all $\chi^2_{\rm d.o.f.}$ values presented in this paper have been computed with the full AP-evolved results, which have an estimated relative error of less than 0.4%.

Our FF exhibit good perturbative stability. In general, there is only little difference between our LO and NLO sets. The only appreciable difference occurs for D_g^K. Since we included in our fit high-quality data from two very different energies, namely 29 and 91.2 GeV, we are sensitive to the running of α_s and are, therefore, able to extract a value of $\Lambda^{(5)}_{\overline{\rm MS}}$, appropriate to five active quark flavours. We find $\Lambda^{(5)}_{\overline{\rm MS}} = 195$ MeV (107 MeV) in NLO (LO), which corresponds to $\alpha_s(M_Z^2) = 0.1154$ (0.1215), in good agreement with the value 0.120 ± 0.008 extracted from a global fit to the Z-boson observables measured at LEP [31]. We find that the error on $\Lambda^{(5)}_{\overline{\rm MS}}$ due to faked scaling effects in connection with the distinct flavour composition at the Z resonance is of the order of 20 MeV. We are quite insensitive to other sources of uncertainties in Λ, such as the one related to the relative normalization of the data.

In this context, we also wish to mention nonperturbative power corrections to the fragmentation process. We assume throughout that such corrections are small and need not be considered when analyzing the presently available data. The good agreement between our results and the various measurements nicely supports this assumption. However, it cannot yet be excluded theoretically that corrections to inclusive timelike processes (such as e^+e^- annihilation) might be of order $1/Q$, which would correspond to a sizeable uncertainty in $\Lambda^{(5)}_{\overline{\rm MS}}$.

Since we have built in the $c\bar{c}$ and $b\bar{b}$ thresholds, we have three different starting scales Q_0. To illustrate the relative size of the FF, we have plotted them in Fig. 1a–d as functions of x for $Q = 10$ GeV. We observe that, in the case of the pion sets, the b-quark distribution is rather soft, whereas the u-quark distribution is quite hard.

The goodness of our fits to the TPC [2] and ALEPH data [14] on charged-pion and -kaon production may be judged from Figs. 2 and 3. The fit to the charged-hadron data by ALEPH is seen in Fig. 4, where we show the contributions due to (1) u, d, s, (2) b, and (3) all flavours. We also compare the contribution due to gluon fragmentation into charged hadrons with the data obtained in the three-jet analysis by OPAL [15]. The full (dotted) curves correspond to our NLO (LO) analysis. In the case of pion and charged-hadron production, our fits describe the data quite well, even for $x < x_{\rm min}$. Specifically, we find $\chi^2_{\rm d.o.f.}$ values of 1.28 (1.32) at NLO (LO), if we include the gluon information. Leaving out the gluon data, we obtain 1.06 (1.14). As may be seen from Table I, the five gluon data points contribute an extraordinarily high value of $\chi^2_{\rm d.o.f.}$.

This concludes the description of our fit procedure and the quality of the fit to the data used. In the next section, we shall first study to what extend our FF also account for other data, both below and at the Z resonance, including the longitudinal cross section at the Z peak, which has recently been measured [13]. In addition, we shall confront our prediction for charged-particle production in ep scattering at HERA with the data by H1 [10] and ZEUS [18].

5 Applications

In order to gain confidence in the validity of our new FF sets, we shall now test them against data which were not used in our fits. Specifically, we shall consider data on charged-pion and -kaon production taken by the DASP [3] and ARGUS Collaborations [4] at DORIS and the TASSO Collaboration [7] at PETRA. Furthermore, we shall make comparisons with charged-hadron data collected by MARK II [5] at PEP, CELLO [6] at PETRA, AMY [8] at TRISTAN, and DELPHI [9] at LEP. In the latter case, we shall assume that the percentage of the produced protons and antiprotons relative to the charged pions may be approximated for all energies by the function $f(x)$ given in Eq. (17), so that Eq. (18) is valid. For each of these data samples, we list in Table I the CM energy, the number of data points with $x_{\min} < x < 0.8$, and the resulting $\chi^2_{\text{d.o.f.}}$ values in NLO and LO. We see that all these data are fitted rather well, with $\chi^2_{\text{d.o.f.}}$ values of the order of unity. In fact, these $\chi^2_{\text{d.o.f.}}$ values are comparable with those we obtained for the TPC [2] and ALEPH [13,14] data, to which we actually fitted. This serves as a nontrivial consistency check for our procedure and tells us that a global fit to all data would not further improve the goodness of our FF. The NLO and LO values of $\chi^2_{\text{d.o.f.}}$ are very similar, with a slight preference for our NLO set. The good agreement with the DASP [3], ARGUS [4], and TASSO [7] data of charged-pion and -kaon production is also demonstrated in Figs. 2 and 3, respectively. The ARGUS data are also very well described for $x < x_{\text{cut}}$. In Fig. 4, we present the comparisons of our theoretical results with the MARK II [5], CELLO [6], and AMY [8] measurements of charged-hadron production. We see from Figs. 2–4 that the LO and NLO calculations agree very well at $\sqrt{s} = 91.2$ GeV, whereas they tend to deviate at smaller energies, the discrepancy being up to 30% at $\sqrt{s} = 5.20$ GeV and medium x.

Another method to extract information on the gluon FF is to analyze the longitudinal cross section $d\sigma^L/dx$ defined in Eq. (2). Similarly the total cross section $d\sigma/dx = d\sigma^T/dx + d\sigma^L/dx$ defined in Eq. (3), which we have considered so far, $d\sigma^L/dx$ may be represented as a convolution of the FF with the longitudinal cross sections of the individual subprocesses given in Eq. (7),

$$\frac{1}{\sigma_{\text{tot}}}\frac{d\sigma^L}{dx} = \frac{\alpha_s}{2\pi}C_F\int_x^1\frac{dz}{z}\left[N_c\frac{\sigma_0}{\sigma_{tot}}\sum_{i=1}^{2N_f}e_{q_i}^2 D_{q_i}^h(z,Q^2) + 4\left(\frac{z}{x}-1\right)D_g^h(z,Q^2)\right] + O(\alpha_s^2). \quad (23)$$

Since Eq. (23) is only given to LO in α_s, the α_s value here is not expected to be the same as the one in the NLO relations (3)–(6). Thus, from measurements of $d\sigma^L/dx$ and $d\sigma^T/dx$, the gluon FF can only be extracted to LO. ALEPH [13] and OPAL [32] have recently presented preliminary data on $d\sigma^L/dx$. In Fig. 5, we evaluate Eq. (23) with our NLO FF and two-loop α_s and compare the result with the ALEPH data [13]. The result obtained (full curve) falls short of the data by a factor of two. At this point, we have to keep in mind that Eq. (23) is a LO prediction, and one should be prepared to allow for a K factor, which is typically larger than one. This K factor may be simulated by changing the renormalization and factorization scales. Assuming a scale of 20 GeV, we are able to nicely describe the data. This comparison provides us with some useful check on the

gluon FF at low x. A similar scale change was considered by Webber in connection with Monte Carlo studies of this observable [32].

In Fig. 4, we compared our analysis with the experimental results on gluon fragmentation into hadrons obtained by OPAL [15] through their three-jet analysis with the corrections of Nason and Webber [15] applied. A more direct comparison with the original OPAL data is feasible. For this purpose, we calculate the ratio of the inclusive scaled energy distribution for gluon-tagged and normal-mixture events, $R_{\mathrm{g.tag/n.mix}}$, as a function of x. This quantity is represented in our analysis by

$$R_{\mathrm{g.tag/n.mix}} = \frac{D_g^h(x,Q^2)\sum_{i=1}^{2N_f} e_i^2}{d\sigma/dx}, \tag{24}$$

where h stands for the sum over the charged hadrons and the quantity in the denominator is defined in Eq. (3). The result of this comparison is presented for LO (dashed line) and NLO (solid line) in Fig. 6. We see that our model gives a good account of $R_{\mathrm{g.tag/n.mix}}$ for medium and large x.

The factorization theorem guarantees that the FF characterize the hadronization phenomena in a process-independent way, *i.e.*, the FF that have been extracted from e^+e^- data may also be used to make predictions for other types of experiments, *e.g.*, at $\gamma\gamma$, ep, and hadron colliders, fixed-target facilities, *etc.* In the following, we shall make NLO predictions for inclusive photoproduction of charged hadrons at HERA and confront them with recent high-statistics data taken by H1 [10] and ZEUS [18]. We shall focus attention on the p_T spectrum of the produced hadrons, averaged over a certain y_{lab} interval. We shall work at NLO in the $\overline{\mathrm{MS}}$ scheme with $N_f = 5$ quark flavours, set $\mu = M_\gamma = M_p = M_h = \xi p_T$, and adopt the photon and proton PDF from Refs. [33] and [34], respectively, along with our FF for charged pions and kaons. Unless stated otherwise, we shall choose $\xi = 1$. We shall evaluate α_s with $\Lambda^{(5)}_{\overline{\mathrm{MS}}} = 158$ MeV [34]. As we have seen in Sect. 3, H1 and ZEUS apply different criteria to select the photoproduction events, which may be simulated by appropriate choices of the photon-energy cuts and the Q^2_{max} value in Eq. (14). Another difference is that the y_{lab} range presently covered by the H1 detector is $-1.5 \le y_{\mathrm{lab}} \le 1.5$, while the ZEUS detector covers $-1.2 \le y_{\mathrm{lab}} \le 1.4$.

In Figs. 7 and 8, we confront the H1 and ZEUS data, respectively, with the corresponding NLO calculations performed with our new FF sets for charged pions and kaons. The agreement is almost perfect for $p_T \lesssim 4$ GeV. For higher values of p_T, the central values of the measurements tend to depart from our predictions in both directions, but, at the same time, the experimental errors become larger. We shall have to await more statistics in the high-p_T range until we can reach final conclusions concerning the agreement of experiment and theory. So far, H1 and ZEUS have not detected separately charged pions and kaons. We would like to take this opportunity and encourage these collaborations to tackle such a separation, since this would allow us to test the factorization theorem of QCD in greater detail. In Fig. 9, we repeat the analyses of Figs. 7 and 8 for the average of the positively- and negatively-charged kaons (dashed lines) and compare the outcome with the full results for H1 and ZEUS shown in Figs. 7 and 8, respectively (solid lines). We see that, in the case of H1 (ZEUS), the ratio of charged kaons to charged

pions ranges between 53% and 70% (54% and 71%) for p_T between 1.5 GeV and 15 GeV. Having gained a solid amount of confidence in the validity of our FF, we may ask the question whether the H1 and ZEUS data already show evidence for the coexistence of the direct- and resolved-photon mechanisms. Toward this end, we compare in Fig. 10 the full calculations of Figs. 7 and 8 with the respective direct-photon contributions. The direct-photon contribution exhibits a discontinuity at $p_T \approx 3$ GeV. This is due to the onset of the charm FF in connection with the $\gamma g \to c\bar{c}$ subprocess, which is not suppressed. In the case of H1 (ZEUS), the direct-photon contribution amounts to between 8% and 48% (9% and 52%) of the total result for p_T between 1.5 GeV and 15 GeV. Also here, we need more statistics at high p_T before we can claim to have detected the direct-photon mechanism in the inclusive photoproduction of hadrons at HERA. Of course, a precise experimental determination of the rapidity distribution for perturbatively high values of p_T would serve as a more direct approach to resolve this issue. The H1 Collaboration has already undertaken a first step in that direction [10]. Another interesting issue is whether the gluon content of the resolved photon has been established by the data. In the case of H1 (ZEUS), it makes up between 67% and 10% (66% and 7%) of the resolved contribution and between 61% and 5% (61% and 3%) of the total one for p_T between 1.5 GeV and 15 GeV. Thus, it seems that, in the absence of the gluon density inside the photon, the theoretical prediction would significantly fall short of the data at low p_T. Again, the shape of the measured rapidity spectrum would serve as an additional discriminator.

Finally, we investigate if our FF satisfy the momentum sum rules. Guided by the idea that a given outgoing parton, a, will fragment with 100% likelihood into some hadron, h, and that momentum is conserved during the fragmentation process, we expect that

$$\sum_h \int_0^1 dx\, x D_a^h(x, Q^2) = 1 \tag{25}$$

holds for any value of Q^2. In our analysis, the left-hand-side of Eq. (25) should be smaller than unity, since we consider only pions, kaons, protons, and antiprotons, which does not exhaust the spectrum of all possible hadrons. We approximate the contributions due to neutral pions, neutral kaons, and protons/antiprotons by

$$D_a^{\pi^0}(x, Q^2) = \frac{1}{2} D_a^{\pi^+ + \pi^-}(x, Q^2), \tag{26}$$

$$D_a^{K^0 + \bar{K}^0}(x, Q^2) = D_a^{K^+ + K^-}(x, Q^2), \tag{27}$$

$$D_a^{p+\bar{p}}(x, Q^2) = f(x) D_a^{\pi^+ + \pi^-}(x, Q^2), \tag{28}$$

respectively, where $f(x)$ was introduced in Eq. (17). Equation (27) is in good agreement with data at various energies [4,35], while Eq. (26) follows on from SU(2) symmetry. We take the lower limit of integration in Eq. (25) to be 0.02. This is presumably too small for the low energies $\sqrt{s} = 2, 4, 10$ GeV, which might explain why the sum-rule values are in some cases larger than one at these energies, in particular for our LO fit. In Table II, we list the results obtained with our LO and NLO FF for $Q = \sqrt{2}$, 5, 10, 91, and 200 GeV. The accuracy of our results is limited due to the uncertainty in the assumptions (26)–(28), and we estimate the error to be of the order of 10%.

TABLE II. Left-hand side of Eq. (25) at NLO for $Q = \sqrt{2}$, 5, 10, 91, and 200 GeV. The numbers in parentheses are evaluated with our LO set. We integrate over $0.02 < x < 0.98$ and sum over pions, kaons, protons, and antiprotons.

a	Q [GeV]				
	$\sqrt{2}$	4	10	91	200
u	0.83 (1.10)	0.86 (1.03)	0.86 (0.98)	0.81 (0.89)	0.79 (0.86)
d	0.95 (1.08)	0.96 (1.02)	0.94 (0.97)	0.88 (0.88)	0.86 (0.85)
s	1.08 (1.70)	1.05 (1.52)	1.02 (1.42)	0.94 (1.23)	0.91 (1.18)
c	–	0.94 (1.14)	0.92 (1.08)	0.86 (0.96)	0.83 (0.92)
b	–	–	0.92 (1.11)	0.85 (0.98)	0.83 (0.94)
g	0.96 (0.93)	0.96 (0.87)	0.91 (0.82)	0.79 (0.70)	0.75 (0.67)

6 Summary and Conclusions

We presented new sets of FF for charged pions and kaons, both at LO and NLO. They were fitted to data on inclusive charged-pion and -kaon production in e^+e^- annihilation taken by TPC [2] at PEP ($\sqrt{s} = 29$ GeV) and by ALEPH [13,14] at LEP. In their charged-hadron sample [13], ALEPH discriminated between events with charm, bottom, and light-flavour fragmentation. This enabled us to treat all partons independently and to properly incorporate the charm and bottom thresholds. We just imposed the conditions $D_d^{\pi^+ + \pi^-} = D_u^{\pi^+ + \pi^-}$ and $D_s^{K^+ + K^-} = D_u^{K^+ + K^-}$, which are quite natural, since we treated the u, d, and s quarks as massless, so that they equally participate in the strong interaction. This constitutes a considerable improvement of our previous analysis [1] based just on the TPC data, where we could only distinguish between valence-quark, sea-quark, and gluon fragmentation and neglected the heavy-flavour thresholds. In order to control the gluon FF, we exploited recent data on inclusive charged-hadron production in tagged three-jet events by OPAL [15] and similar data for longitudinal electron polarization by ALEPH [13]. Due to the sizeable energy gap between PEP and LEP, we were also sensitive to the scaling violation in the fragmentation process. This allowed us to extract a value for $\Lambda^{(5)}_{\overline{\rm MS}}$. We found $\Lambda^{(5)}_{\overline{\rm MS}} = 195$ MeV (107 MeV) in NLO (LO), in good agreement with the global analysis of LEP data [31].

Although our FF were only fitted to the TPC [2] and ALEPH data [13,14], it turned out that they lead to an excellent description of a wealth of other e^+e^- data on inclusive charged-hadron production, ranging from $\sqrt{s} = 5.2$ GeV to LEP energy [3,4,5,6,7,8,9]. In fact, we always obtained $\chi^2_{\rm d.o.f.}$ values of order unity. The only exception, with $\chi^2_{\rm d.o.f.} \approx 9$, occurred in the longitudinal cross section [13], which is of $O(\alpha_s)$ and suffers from a considerable scale ambiguity.

In order to test quantitatively the factorization theorem of fragmentation in the QCD-improved parton model at the quantum level, we made NLO predictions for the p_T spectrum of charged hadrons produced inclusively in the scattering of quasi-real photons on protons under HERA conditions, and confronted them with new high-statistics data by H1 [10] and ZEUS [18]. Also here, the outcome of the comparison was very encouraging,

especially in the lower p_T range, where the experimental errors are smallest. We found first evidence for the interplay between the direct- and resolved-photon mechanisms in the inclusive photoproduction of hadrons. Our comparisons also support the notion that, during a fraction of time, the photon can interact with the partons inside the proton like a gluon.

ACKNOWLEDGMENTS

We thank Glen Cowan and Cristobal Padilla for detailed information on Ref. [13]. Furthermore, we thank Michal Kasprzak for making available to us the latest ZEUS data on inclusive photoproduction of charged hadrons prior to their official publication [18]. One of us (GK) thanks the Theory Group of the Werner-Heisenberg-Institut for the hospitality extended to him during a visit when this paper was finalized.

A Parameterizations

For the reader's convenience, we shall present here simple parameterizations of the x and Q^2 dependence of our FF.[2] As usual, we introduce the scaling variable

$$\bar{s} = \ln \frac{\ln\left(Q^2/\Lambda^2\right)}{\ln\left(Q_0^2/\Lambda^2\right)}. \tag{29}$$

For Λ we use the $\overline{\rm MS}$ value appropriate to $N_f = 5$ flavours, since the parameterization would not benefit from the incorporation of discontinuities in $\bar{s}$. $\Lambda^{(5)}_{\overline{\rm MS}}$ is determined from our fit to be 107 MeV (195 MeV) in LO (NLO). Similarly to Eqs. (19)–(22), we use three different values for Q_0, namely

$$Q_0 \;=\; \begin{cases} \sqrt{2}\ \text{GeV}, & \text{if} \quad a = u, d, s, g \\ m(\eta_c) = 2.9788\ \text{GeV}, & \text{if} \quad a = c \\ m(\Upsilon) = 9.46037\ \text{GeV}, & \text{if} \quad a = b \end{cases} . \tag{30}$$

This leads to three different definitions of $\bar{s}$. For definiteness, we use the symbol $\bar{s}_c$ for charm and $\bar{s}_b$ for bottom along with $\bar{s}$ for the residual partons.

We parameterize our FF by simple functions in x with coefficients which we write as polynomials in $\bar{s}$, $\bar{s}_c$, and $\bar{s}_b$. We find that the template

$$D(x, Q^2) = N x^\alpha (1-x)^\beta \tag{31}$$

is sufficiently flexible, except for $D_b^{(\pi,LO)}$, $D_b^{(\pi,NLO)}$, and $D_g^{(K,NLO)}$, where we include an additional factor $(1 + \gamma/x)$ on the right-hand side of Eq. (31). For $\bar{s} = \bar{s}_c = \bar{s}_b = 0$, the parameterizations agree with the respective ansätze in Eqs. (19)–(22). The charm and bottom parameterizations must be put to zero by hand for $\bar{s}_c < 0$ and $\bar{s}_b < 0$, respectively.

[2] A FORTRAN subroutine that returns the FF for given x and Q^2 may be obtained from the authors via e-mail (binnewie@ips107.desy.de, kniehl@vms.mppmu.mpg.de).

We list below the parameters to be inserted in Eq. (31) for charged pions and kaons both at LO and NLO. The resulting parameterizations correctly describe the AP evolution up to 10% for $Q_0 \leq Q \leq 150$ GeV and $x \geq 0.1$. Deviations in excess of 10% may occur for $x < 0.1$.

1. LO FF for $(\pi^+ + \pi^-)$:

   - $D_u^{(\pi,LO)}(x,Q^2) = D_d^{(\pi,LO)}(x,Q^2)$:

$$\begin{aligned} N &= 1.090 - 1.085\bar{s} + 0.700\bar{s}^2 - 0.217\bar{s}^3 \\ \alpha &= -0.842 - 0.920\bar{s} + 0.532\bar{s}^2 - 0.148\bar{s}^3 \\ \beta &= 1.430 + 0.434\bar{s} + 0.035\bar{s}^2 + 0.060\bar{s}^3 \end{aligned} \tag{32}$$

   - $D_s^{(\pi,LO)}(x,Q^2)$:

$$\begin{aligned} N &= 3.470 - 2.340\bar{s} + 0.309\bar{s}^2 + 0.120\bar{s}^3 \\ \alpha &= -1.037 - 0.301\bar{s} - 0.038\bar{s}^2 + 0.031\bar{s}^3 \\ \beta &= 3.880 + 0.866\bar{s} - 0.137\bar{s}^2 + 0.058\bar{s}^3 \end{aligned} \tag{33}$$

   - $D_c^{(\pi,LO)}(x,Q^2)$:

$$\begin{aligned} N &= 4.520 - 3.966\bar{s}_c + 1.453\bar{s}_c^2 - 0.261\bar{s}_c^3 \\ \alpha &= -0.898 - 0.382\bar{s}_c + 0.027\bar{s}_c^3 \\ \beta &= 4.690 + 0.742\bar{s}_c \end{aligned} \tag{34}$$

   - $D_b^{(\pi,LO)}(x,Q^2)$:

$$\begin{aligned} N &= 3.620 - 9.669\bar{s}_b + 13.160\bar{s}_b^2 - 5.406\bar{s}_b^3 \\ \alpha &= -1.128 - 1.613\bar{s}_b + 2.715\bar{s}_b^3 \\ \beta &= 7.120 - 1.081\bar{s}_b + 0.936\bar{s}_b^2 + 1.678\bar{s}_b^3 \\ \gamma &= -0.164\bar{s}_b + 0.208\bar{s}_b^2 \end{aligned} \tag{35}$$

   - $D_g^{(\pi,LO)}(x,Q^2)$:

$$\begin{aligned} N &= 6.200 - 13.100\bar{s} + 10.940\bar{s}^2 - 3.395\bar{s}^3 \\ \alpha &= -0.351 - 1.542\bar{s} + 0.319\bar{s}^2 + 0.074\bar{s}^3 \\ \beta &= 3.000 + 1.567\bar{s} - 0.725\bar{s}^2 + 0.465\bar{s}^3 \end{aligned} \tag{36}$$

2. NLO FF for $(\pi^+ + \pi^-)$:

   - $D_u^{(\pi,NLO)}(x,Q^2) = D_d^{(\pi,NLO)}(x,Q^2)$:

$$\begin{aligned} N &= 1.160 - 1.292\bar{s} + 0.975\bar{s}^2 - 0.341\bar{s}^3 \\ \alpha &= -0.762 - 1.392\bar{s} + 1.151\bar{s}^2 - 0.429\bar{s}^3 \\ \beta &= 1.470 + 0.752\bar{s} - 0.350\bar{s}^2 + 0.175\bar{s}^3 \end{aligned} \tag{37}$$

- $D_s^{(\pi,NLO)}(x,Q^2)$:

$$\begin{aligned} N &= 3.960 - 3.148\bar{s} + 1.198\bar{s}^2 - 0.267\bar{s}^3 \\ \alpha &= -0.825 - 0.552\bar{s} + 0.206\bar{s}^2 - 0.070\bar{s}^3 \\ \beta &= 4.380 + 0.940\bar{s} - 0.245\bar{s}^2 + 0.082\bar{s}^3 \end{aligned} \tag{38}$$

- $D_c^{(\pi,NLO)}(x,Q^2)$:

$$\begin{aligned} N &= 3.690 - 3.285\bar{s}_c + 1.383\bar{s}_c^2 - 0.305\bar{s}_c^3 \\ \alpha &= -0.873 - 0.481\bar{s}_c + 0.085\bar{s}_c^2 \\ \beta &= 5.060 + 0.685\bar{s}_c - 0.032\bar{s}_c^2 + 0.038\bar{s}_c^3 \end{aligned} \tag{39}$$

- $D_b^{(\pi,NLO)}(x,Q^2)$:

$$\begin{aligned} N &= 4.000 - 12.965\bar{s}_b + 18.913\bar{s}_b^2 - 10.853\bar{s}_b^3 \\ \alpha &= -1.037 - 1.705\bar{s}_b - 0.865\bar{s}_b^2 + 1.423\bar{s}_b^3 \\ \beta &= 7.750 - 2.306\bar{s}_b + 1.877\bar{s}_b^2 + 0.044\bar{s}_b^3 \\ \gamma &= -0.116\bar{s}_b \end{aligned} \tag{40}$$

- $D_g^{(\pi,NLO)}(x,Q^2)$:

$$\begin{aligned} N &= 5.110 - 9.419\bar{s} + 7.144\bar{s}^2 - 2.069\bar{s}^3 \\ \alpha &= -0.287 - 2.011\bar{s} + 1.211\bar{s}^2 - 0.377\bar{s}^3 \\ \beta &= 2.610 + 2.336\bar{s} - 1.580\bar{s}^2 + 0.756\bar{s}^3 \end{aligned} \tag{41}$$

3. LO FF for $(K^+ + K^-)$:

- $D_u^{(K,LO)}(x,Q^2) = D_s^{(K,LO)}(x,Q^2)$:

$$\begin{aligned} N &= 0.380 - 0.123\bar{s} - 0.015\bar{s}^2 + 0.010\bar{s}^3 \\ \alpha &= -1.234 - 0.106\bar{s} - 0.035\bar{s}^2 + 0.011\bar{s}^3 \\ \beta &= 1.040 + 0.708\bar{s} - 0.086\bar{s}^2 + 0.048\bar{s}^3 \end{aligned} \tag{42}$$

- $D_d^{(K,LO)}(x,Q^2)$:

$$\begin{aligned} N &= 1.110 - 0.674\bar{s} + 0.095\bar{s}^2 + 0.028\bar{s}^3 \\ \alpha &= -0.942 - 0.214\bar{s} - 0.067\bar{s}^2 + 0.041\bar{s}^3 \\ \beta &= 2.810 + 0.852\bar{s} - 0.172\bar{s}^2 + 0.090\bar{s}^3 \end{aligned} \tag{43}$$

- $D_c^{(K,LO)}(x,Q^2)$:

$$\begin{aligned} N &= 0.550 - 0.392\bar{s}_c + 0.088\bar{s}_c^2 \\ \alpha &= -0.764 - 0.378\bar{s}_c \\ \beta &= 2.690 + 0.713\bar{s}_c - 0.103\bar{s}_c^2 + 0.064\bar{s}_c^3 \end{aligned} \tag{44}$$

- $D_b^{(K,LO)}(x,Q^2)$:

$$\begin{aligned} N &= 0.720 - 0.495\bar{s}_b + 0.205\bar{s}_b^3 \\ \alpha &= -0.792 - 0.296\bar{s}_b - 0.261\bar{s}_b^2 + 0.421\bar{s}_b^3 \\ \beta &= 2.810 + 0.686\bar{s}_b \end{aligned} \tag{45}$$

- $D_g^{(K,LO)}(x,Q^2)$:

$$\begin{aligned} N &= 0.430 - 0.915\bar{s} + 0.885\bar{s}^2 - 0.316\bar{s}^3 \\ \alpha &= -0.374 - 2.368\bar{s} + 1.475\bar{s}^2 - 0.317\bar{s}^3 \\ \beta &= 2.690 + 1.137\bar{s} - 0.934\bar{s}^2 + 0.698\bar{s}^3 \end{aligned} \tag{46}$$

4. NLO FF for $(K^+ + K^-)$:

- $D_u^{(K,NLO)}(x,Q^2) = D_s^{(K,NLO)}(x,Q^2)$:

$$\begin{aligned} N &= 0.300 + 0.039\bar{s} - 0.189\bar{s}^2 + 0.070\bar{s}^3 \\ \alpha &= -0.978 - 0.304\bar{s} - 0.004\bar{s}^2 - 0.004\bar{s}^3 \\ \beta &= 1.010 + 1.193\bar{s} - 0.654\bar{s}^2 + 0.223\bar{s}^3 \end{aligned} \tag{47}$$

- $D_d^{(K,NLO)}(x,Q^2)$:

$$\begin{aligned} N &= 1.050 - 0.546\bar{s} + 0.071\bar{s}^2 + 0.009\bar{s}^3 \\ \alpha &= -0.804 - 0.347\bar{s} + 0.023\bar{s}^2 + 0.007\bar{s}^3 \\ \beta &= 2.540 + 0.919\bar{s} - 0.321\bar{s}^2 + 0.138\bar{s}^3 \end{aligned} \tag{48}$$

- $D_c^{(K,NLO)}(x,Q^2)$:

$$\begin{aligned} N &= 0.680 - 0.415\bar{s}_c + 0.092\bar{s}_c^2 \\ \alpha &= -0.753 - 0.484\bar{s}_c + 0.099\bar{s}_c^2 \\ \beta &= 2.590 + 0.661\bar{s}_c \end{aligned} \tag{49}$$

- $D_b^{(K,NLO)}(x,Q^2)$:

$$\begin{aligned} N &= 0.580 - 0.381\bar{s}_b + 0.114\bar{s}_b^3 \\ \alpha &= -0.843 - 0.414\bar{s}_b - 0.120\bar{s}_b^2 + 0.242\bar{s}_b^3 \\ \beta &= 2.880 + 0.614\bar{s}_b \end{aligned} \tag{50}$$

- $D_g^{(K,NLO)}(x,Q^2)$:

$$\begin{aligned} N &= 0.330 - 0.196\bar{s} - 0.056\bar{s}^2 + 0.057\bar{s}^3 \\ \alpha &= -0.351 - 0.026\bar{s} - 0.480\bar{s}^2 + 0.148\bar{s}^3 \\ \beta &= 0.650 + 2.326\bar{s} - 0.840\bar{s}^2 + 0.314\bar{s}^3 \\ \gamma &= 1.033\bar{s} - 0.479\bar{s}^2 \end{aligned} \tag{51}$$

References

[1] J. Binnewies, B.A. Kniehl, and G. Kramer, Z. Phys. C **65**, 471 (1995).

[2] TPC Collaboration, H. Aihara *et al.*, LBL Report No. LBL-23737 (1988).

[3] DASP Collaboration, R. Brandelik *et al.*, Nucl. Phys. **B148**, 189 (1979).

[4] ARGUS Collaboration, H. Albrecht *et al.*, Z. Phys. C **44**, 547 (1989).

[5] MARK II Collaboration, A. Peterson *et al.*, Phys. Rev. D **37**, 1 (1988).

[6] CELLO Collaboration, H.J. Behrend *et al.*, to be published. The data were taken from Ref. [9].

[7] TASSO Collaboration, W. Braunschweig *et al.*, Z. Phys. C **42**, 182 (1989).

[8] AMY Collaboration, Y.K. Li *et al.*, Phys. Rev. D **41**, 2675 (1990).

[9] DELPHI Collaboration, P. Abreu *et al.*, Phys. Lett. B **311**, 408 (1993).

[10] H1 Collaboration, I. Abt *et al.*, Phys. Lett. B **328**, 176 (1994).

[11] B.A. Kniehl, in *Proceedings of the Workshop on Two-Photon Physics at LEP and HERA*, Lund, Sweden, May 26–28, 1994, edited by G. Jarlskog and L. Jönsson (Krontryck, Eslöv, 1994), p. 264.

[12] F.M. Borzumati and G. Kramer, Report Nos. DESY 95–020, TUM–T31–84/95, hep–ph/9502280 (January 1995).

[13] G.D. Cowan, Siegen University Report No. Si–94–12, to appear in *Proceedings of the 27th International Conference on High Energy Physics*, Glasgow, Scotland, July 20–27, 1994; private communication; C. Padilla, private communication. Data on σ^L were also taken by the OPAL Collaboration and were presented in Ref. [32].

[14] ALEPH Collaboration, D. Buskulic *et al.*, CERN Report No. CERN–PPE/94–201 (December 1994). Compatible data were published by the OPAL Collaboration, P.D. Acton *et al.*, Z. Phys. C **63**, 181 (1994).

[15] OPAL Collaboration, P.D. Acton *et al.*, Z. Phys. C **58**, 387 (1993). Corrections to $D_g(x)$ were applied by P. Nason and B.R. Webber, Nucl. Phys. **B421**, 473 (1994).

[16] OPAL Collaboration, P.D. Acton *et al.*, Z. Phys. C **61**, 209 (1994); DELPHI Collaboration, P. Abreu *et al.*, Phys. Lett. B **347**, 447 (1995).

[17] V.N. Gribov and L.N. Lipatov, Yad. Fiz. **15**, 781 (1972) [Sov. J. Nucl. Phys. **15**, 438 (1972)]; G. Altarelli and G. Parisi, Nucl. Phys. **B126**, 298 (1977); Yu.L. Dokshitser, Zh. Eksp. Teor. Fiz. **73**, 1216 (1977) [Sov. Phys. JETP **46**, 641 (1977)].

[18] M. Kasprzak, private communication; ZEUS Collaboration, M. Derrick *et al.*, DESY Report No. 95–050 (March 1995).

[19] G. Altarelli, R.K. Ellis, G. Martinelli, and S.Y. Pi, Nucl. Phys. **B160**, 301 (1979); R. Baier and K. Fey, Z. Phys. C **2**, 339 (1979).

[20] Particle Data Group, L. Montanet *et al.*, Phys. Rev. D **45**, 1173 (1992).

[21] G. Curci, W. Furmanski, and R. Petronzio, Nucl. Phys. **B175**, 27 (1980); W. Furmanski and R. Petronzio, Phys. Lett. **97B**, 437 (1980); Z. Phys. C **11**, 293 (1982).

[22] E.G. Floratos, C. Kounnas, and R. Lacaze, Nucl. Phys. **B192**, 417 (1981).

[23] M. Glück, E. Reya, and A. Vogt, Phys. Rev. D **48**, 116 (1993).

[24] A. Rostovtsev and V. Soloshenko, H1 Note H1–08/93-309 (August 1993); S. Frixione, M.L. Mangano, P. Nason, and G. Ridolfi, Phys. Lett. B **319**, 339 (1993).

[25] F. Aversa, P. Chiappetta, M. Greco, and J.Ph. Guillet, Phys. Lett. B **210**, 225 (1988); *ibid.* **211**, 465 (1988); Nucl. Phys. **B327**, 105 (1989).

[26] B.A. Kniehl and G. Kramer, Z. Phys. C **62**, 53 (1994).

[27] P. Aurenche, R. Baier, A. Douiri, M. Fontannaz, and D. Schiff, Nucl. Phys. **B286**, 553 (1987).

[28] L.E. Gordon, Phys. Rev. D **50**, 6753 (1994).

[29] F.M. Borzumati, B.A. Kniehl, and G. Kramer, Z. Phys. C **59**, 341 (1993); M. Greco, S. Rolli, and A. Vicini, *ibid.* **65**, 277 (1995).

[30] MINUIT, CERN Computer Centre Program Library.

[31] T. Hebbeker, M. Martinez, G. Passarino, and G. Quast, Phys. Lett. B **331**, 165 (1994).

[32] B.R. Webber, Cavendish Laboratory Report Nos. CAVENDISH-HEP-94-17, hep–ph/9411384 (November 1994).

[33] M. Glück, E. Reya, and A. Vogt, Phys. Rev. D **46**, 1973 (1992).

[34] H.L. Lai, J. Botts, J. Huston, J.G. Morfin, J.F. Owens, J.W. Qiu, W.K. Tung, and H. Weerts, Michigan State University Report Nos. MSU–HEP–41024, hep–ph/9410404 (October 1994); W.K. Tung, private communication.

[35] TASSO Collaboration, W. Braunschweig *et al.*, Z. Phys. C **47**, 167 (1990); ALEPH Collaboration, D. Buskulic *et al.*, *ibid.* **64**, 361 (1994).

FIGURE CAPTIONS

Figure 1: x dependence of the FF at $Q^2 = 100$ GeV^2 for (a) charged pions at NLO, (b) charged pions at LO, (c) charged kaons at NLO, and (d) charged kaons at LO.

Figure 2: Differential cross section of inclusive charged-pion production at LO (dashed lines) and NLO (solid lines) as a function of x at $\sqrt{s} = 5.2$ [3], 9.98 [4], 29 [2], 34 [7], and 91.2 GeV [14]. Upper curves correspond to lower energies. The theoretical calculations are compared with the respective experimental data.

Figure 3: Same as in Fig. 2 for charged kaons.

Figure 4: Differential cross section of inclusive charged-hadron production at LO (dashed lines) and NLO (solid lines) as a function of x at $\sqrt{s} = 29$ [5], 35 [6], 55.2 [8], and 91.2 GeV [13,15]. Upper curves correspond to lower energies. The downmost four curves all refer to LEP energy. The second and third of them correspond to the contributions due to the u, d, s quarks and the b quark [13], respectively. The fourth spectrum shows the x dependence of the gluon FF as measured by OPAL [15]. The theoretical calculations are compared with the respective experimental data.

Figure 5: Differential longitudinal cross section of inclusive charged-hadron production at NLO as a function of x at $\sqrt{s} = 91.2$ GeV. The dashed line is obtained by choosing the renormalization and fragmentation scales to be 20 GeV. The theoretical calculations are compared with the experimental data [13].

Figure 6: Ratio of the inclusive scaled energy distribution for gluon-tagged and normal-mixture events at LO (dashed line) and NLO (solid line) as a function of x for $\sqrt{s} = 91.2$ GeV. The theoretical calculations are compared with the experimental data [15].

Figure 7: The p_T spectrum of inclusive charged-hadron production as measured by ZEUS [18] is compared with the NLO calculation in the $\overline{\rm MS}$ scheme with $N_f = 5$ flavours using the photon and proton PDF of Refs. [33] and [34], respectively. The dashed/solid/dotted curves correspond to the choices $\xi = 0.5/1/2$.

Figure 8: Same as in Fig. 7 for H1 [10].

Figure 9: Comparison of the charged-kaon contributions (dashed lines) with the full results (solid lines) for the theoretical calculations in Figs. 7 and 8. For better separation, the charged-kaon contributions are divided by a factor of two. The upper (lower) curves correspond to H1 (ZEUS) conditions.

Figure 10: Comparison of the direct-photon contributions (dashed lines) with the full results (solid lines) for the theoretical calculations in Figs. 7 and 8. The steps in the direct-photon contributions are due to the opening of the $\gamma g \to c\bar{c}$ subprocess at the charm-quark threshold. The upper (lower) curves correspond to H1 (ZEUS) conditions.

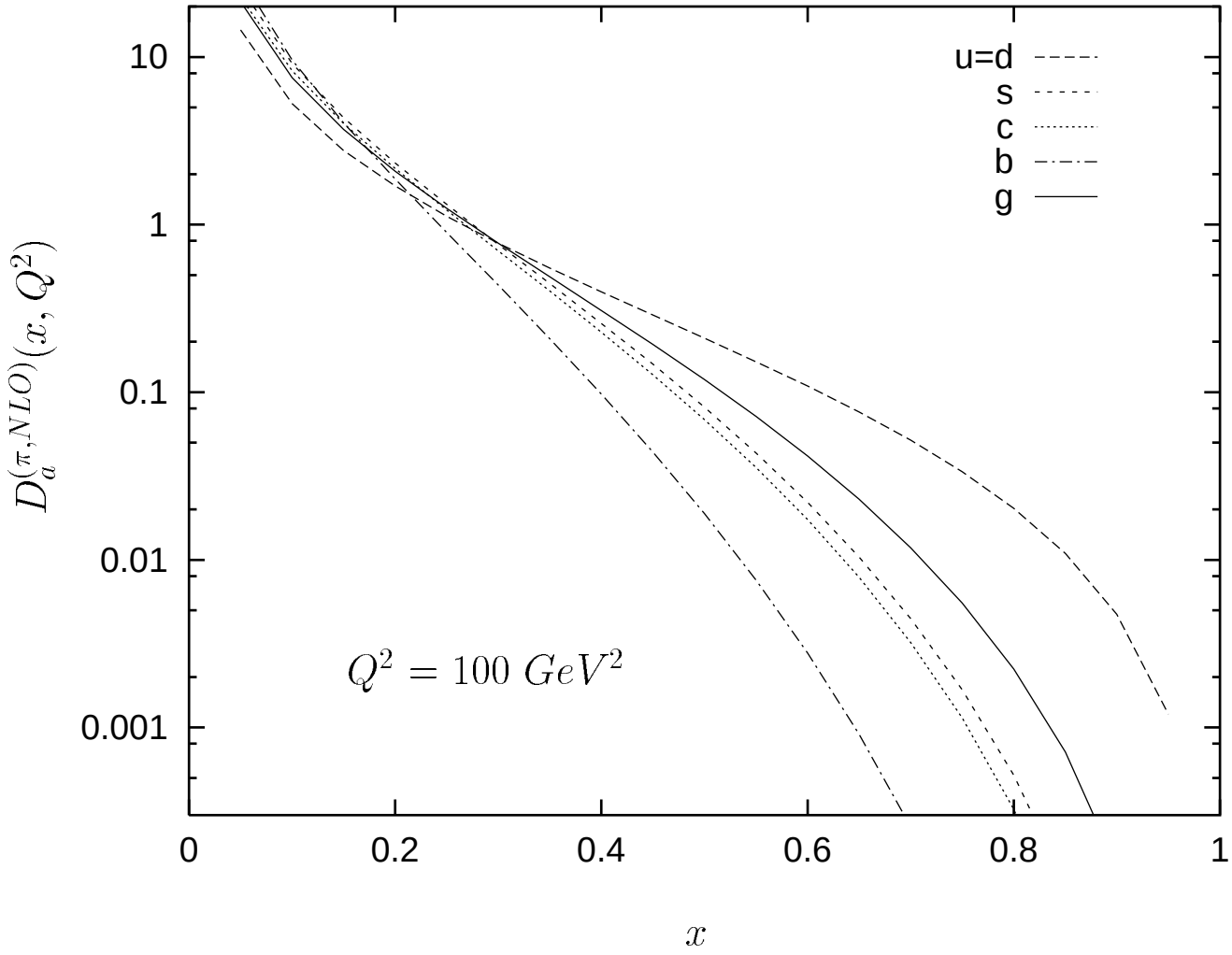

Fig. 1a

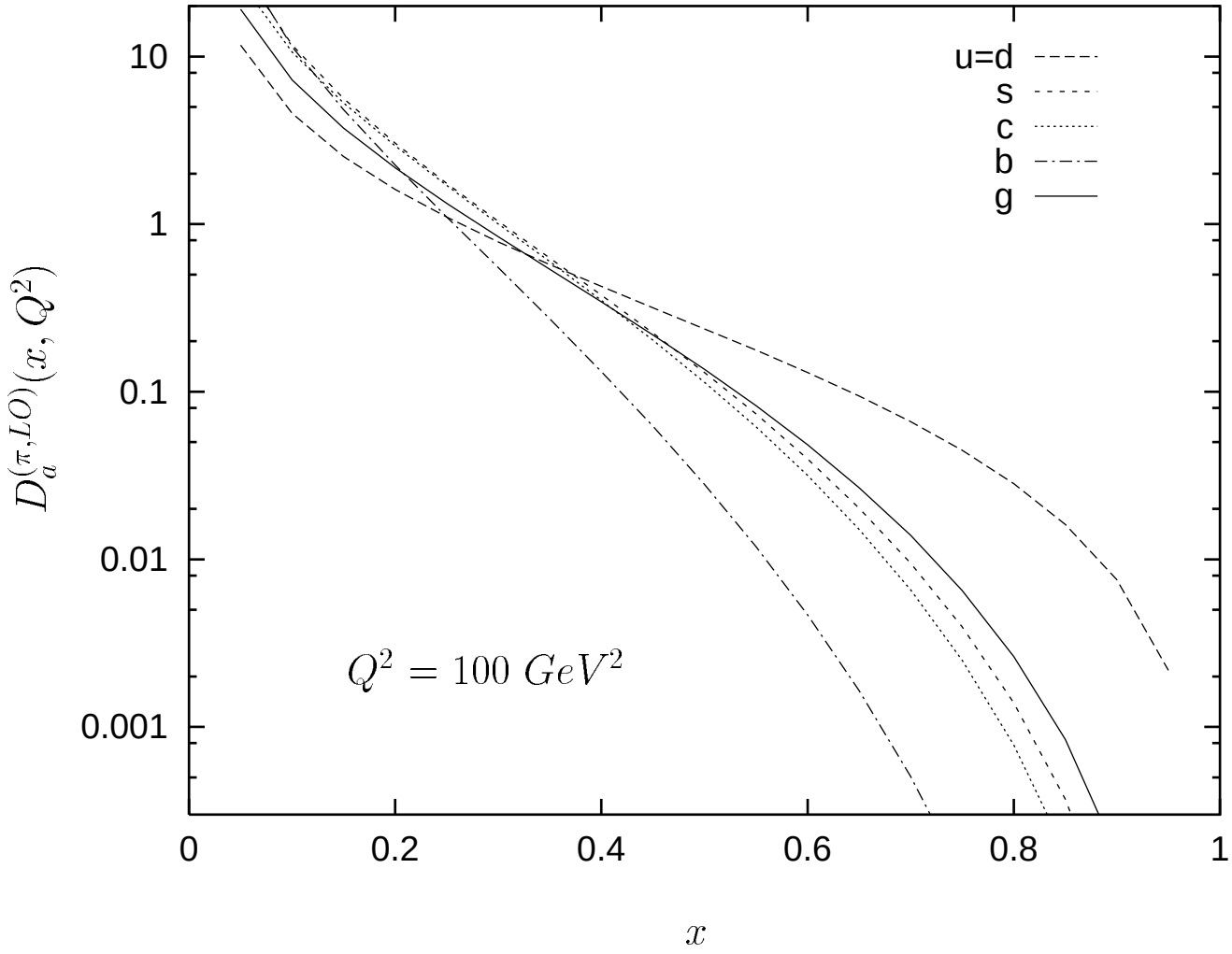

Fig. 1b

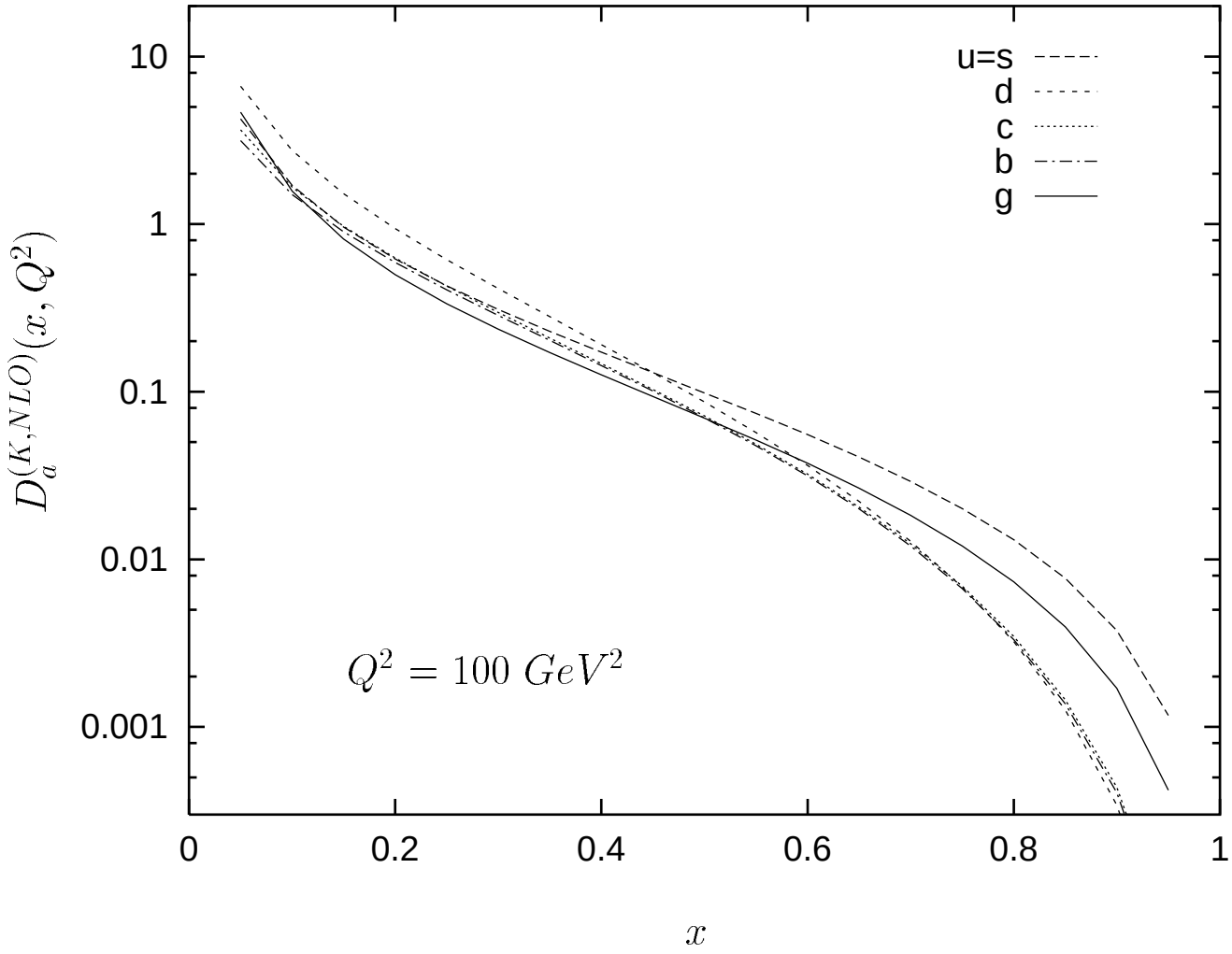

Fig. 1c

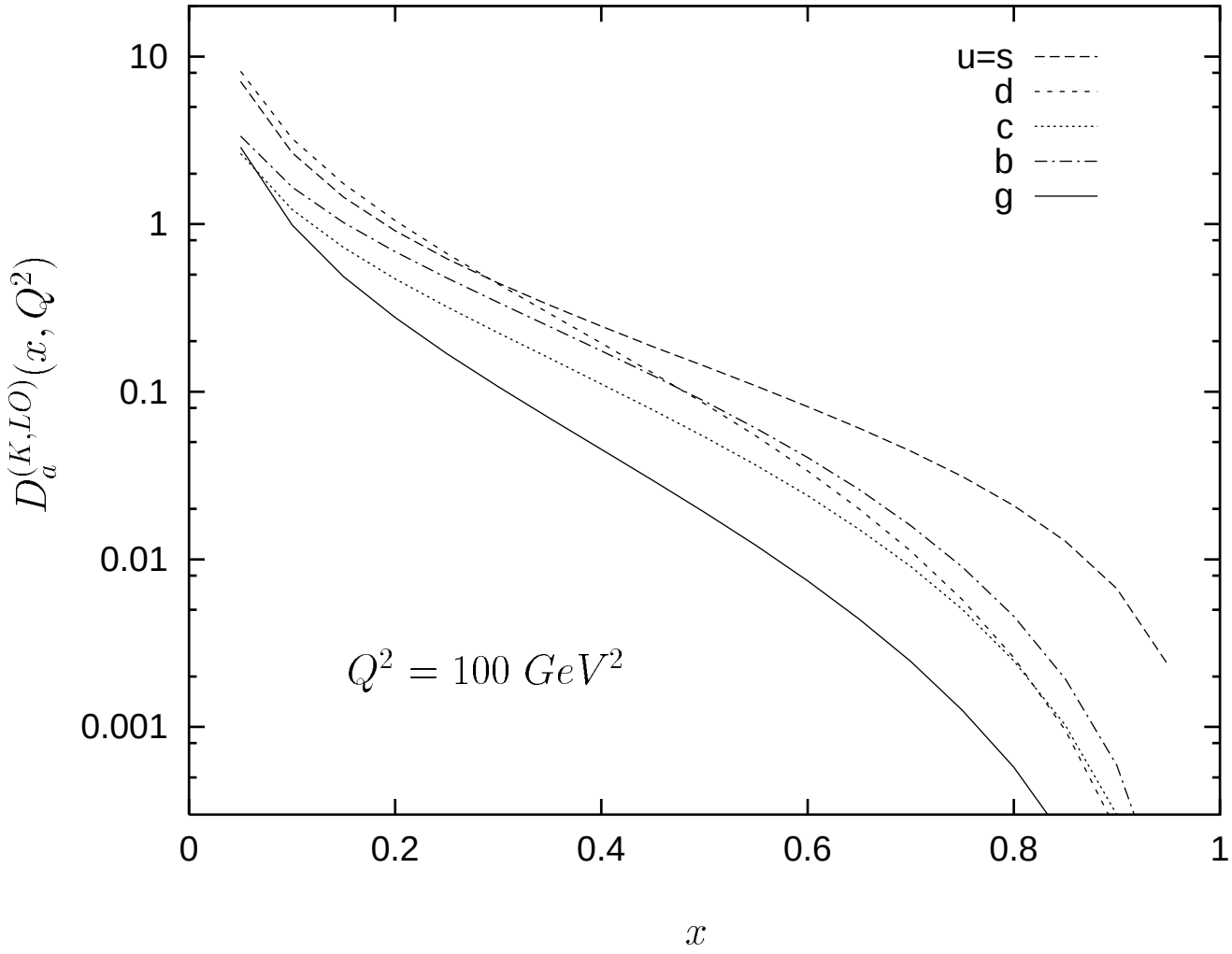

Fig. 1d

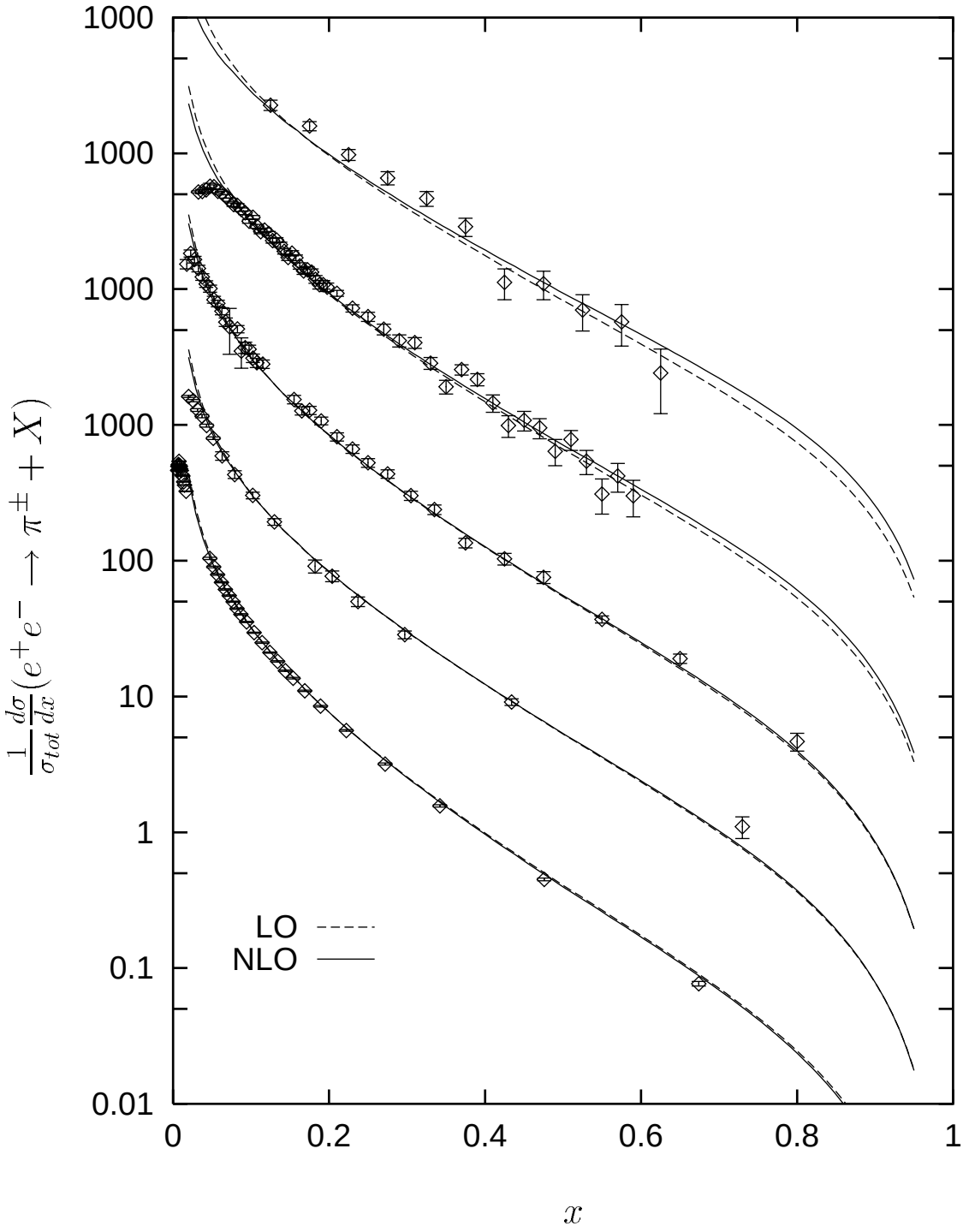
1000
1000
1000
100
10
1
0.1
0.01
0
0.2
0.4
0.6
0.8
1
LO
NLO
$\frac{1}{\sigma_{tot}}\frac{d\sigma}{dx}(e^+e^- \to \pi^\pm + X)$
x

Fig. 2

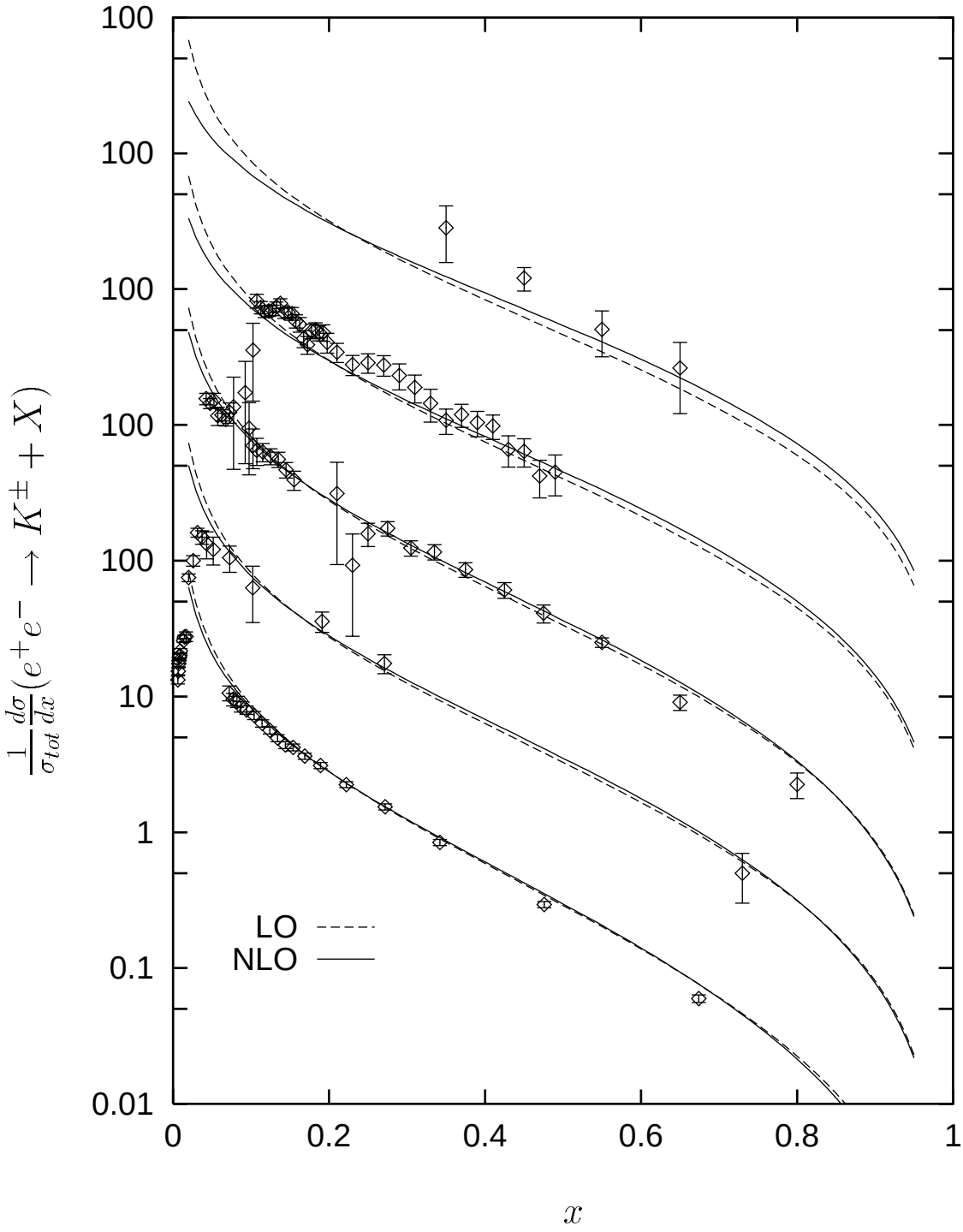
100
100
100
100
10
1
0.1
0.01
0
0.2
0.4
0.6
0.8
1
LO
NLO
$\frac{1}{\sigma_{tot}}\frac{d\sigma}{dx}(e^+e^- \to K^\pm + X)$
x

Fig. 3

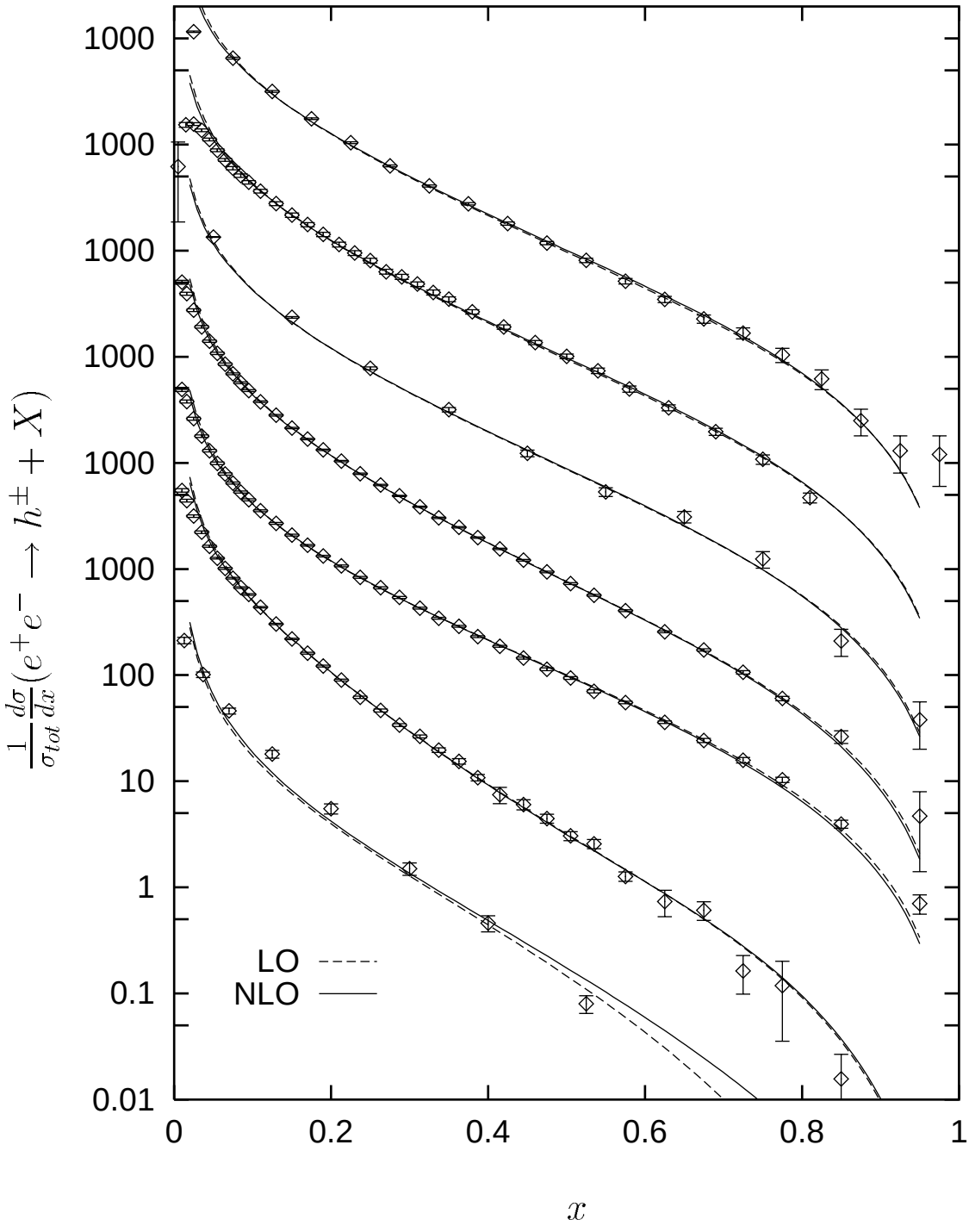
1000
1000
1000
1000
1000
100
10
1
0.1
0.01
0
0.2
0.4
0.6
0.8
1
LO
NLO
$\frac{1}{\sigma_{tot}}\frac{d\sigma}{dx}(e^+e^- \to h^\pm + X)$
x

Fig. 4

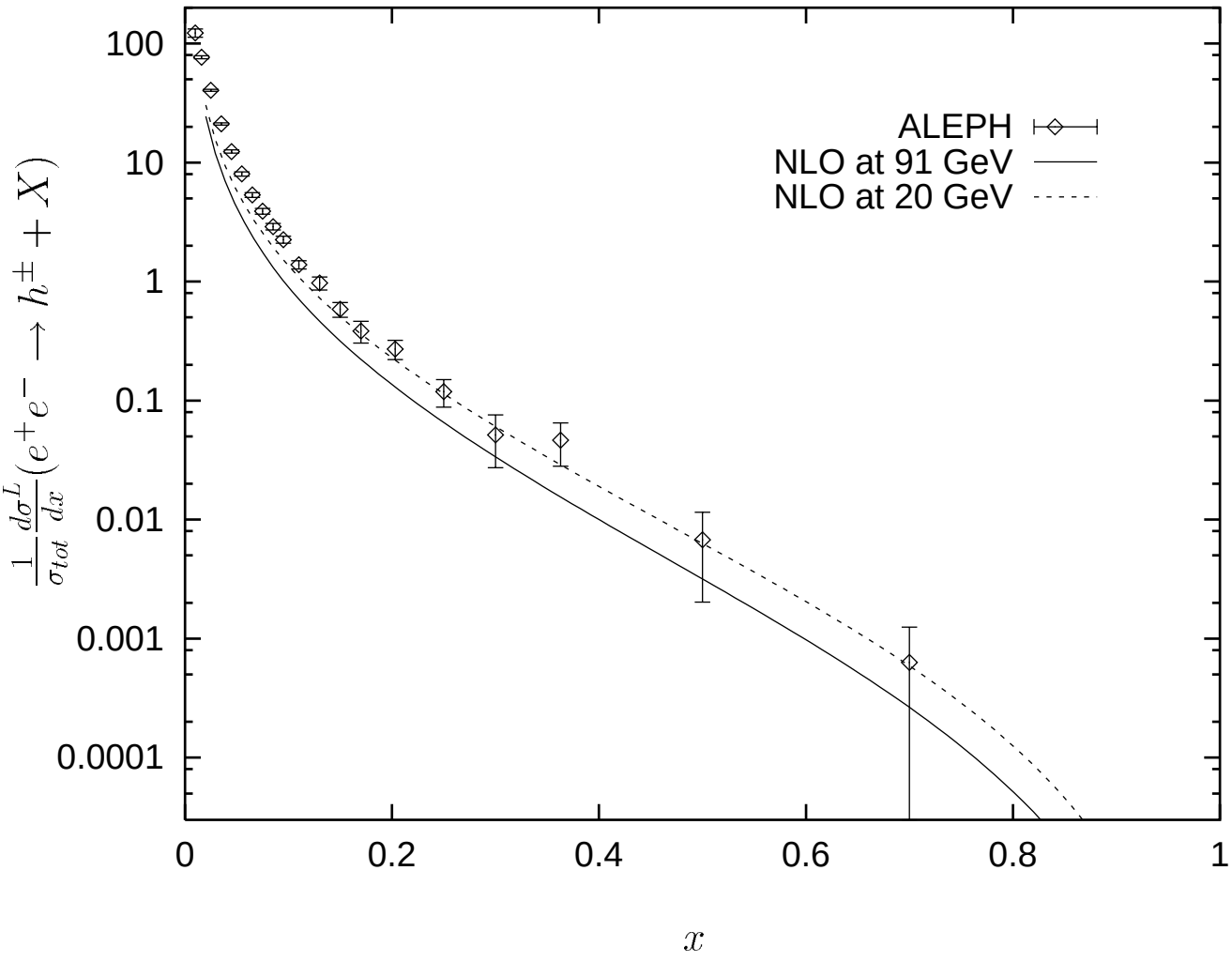
ALEPH
NLO at 91 GeV
NLO at 20 GeV
100
10
1
0.1
0.01
0.001
0.0001
0
0.2
0.4
0.6
0.8
1
$\frac{1}{\sigma_{tot}}\frac{d\sigma^L}{dx}(e^+e^- \to h^\pm + X)$
x

Fig. 5

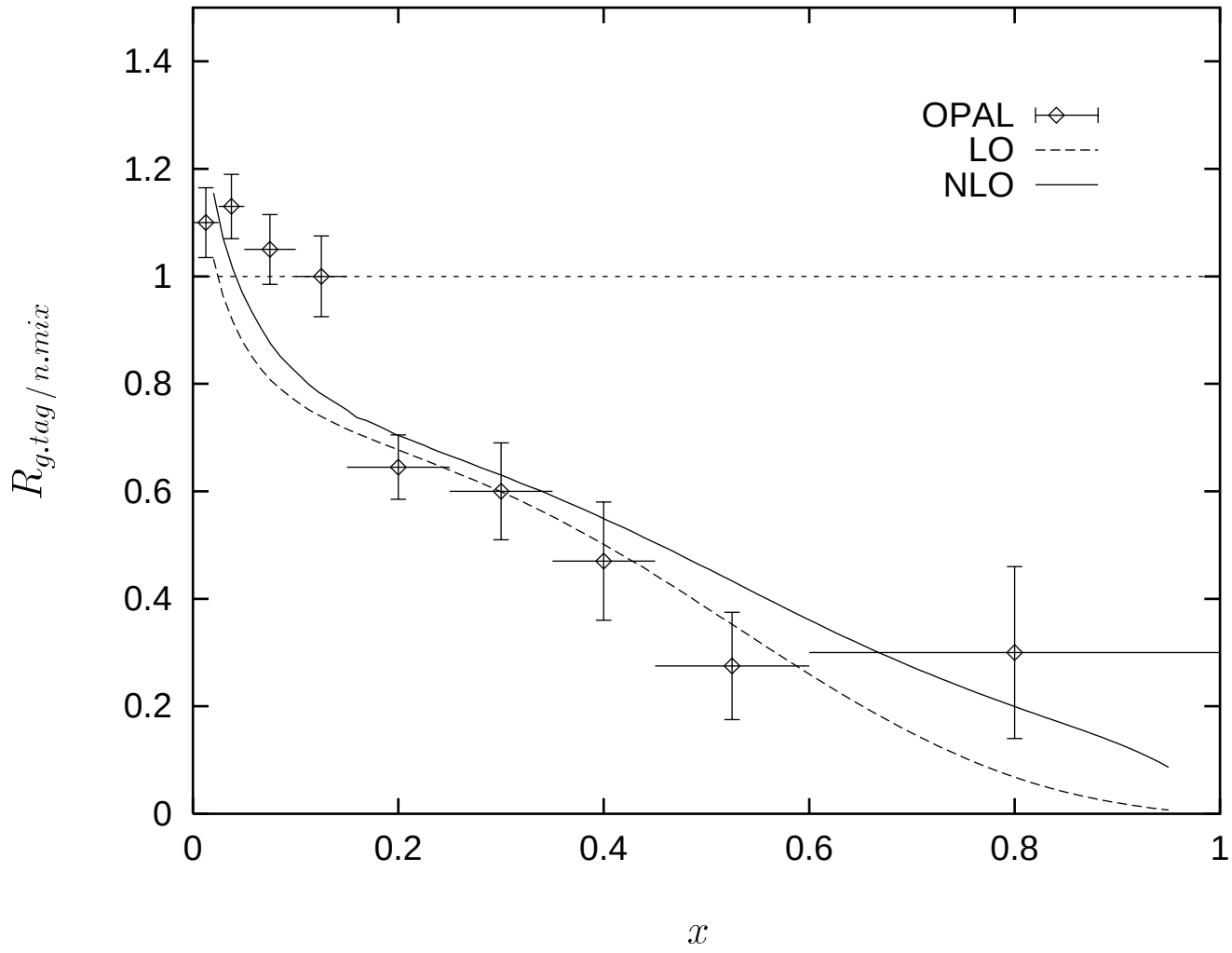

Fig. 6

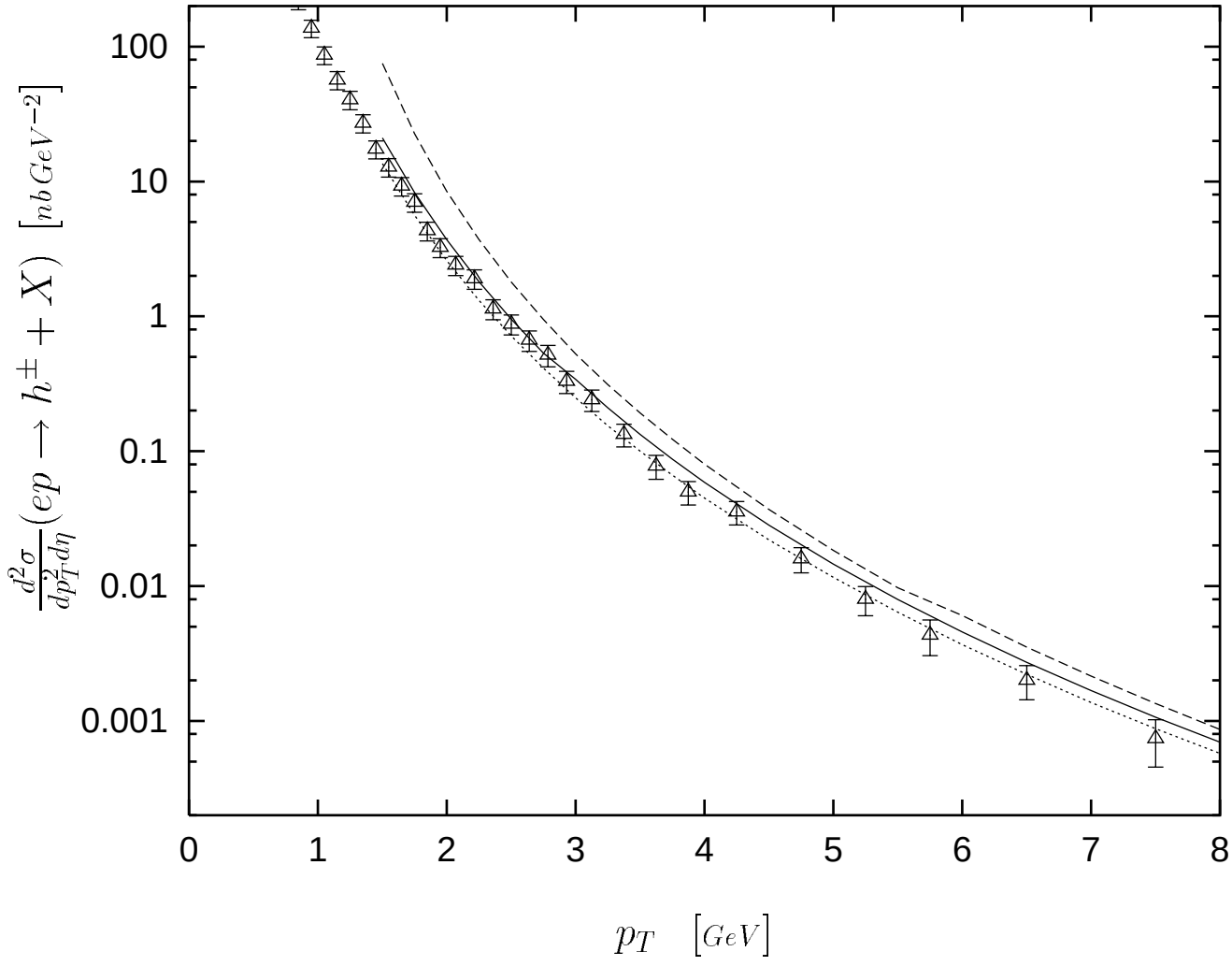
100
10
1
0.1
0.01
0.001
0
1
2
3
4
5
6
7
8
$\frac{d^2\sigma}{dp_T^2 d\eta}(ep \to h^{\pm} + X)$ $[nb\,GeV^{-2}]$
p_T $[GeV]$

Fig. 7

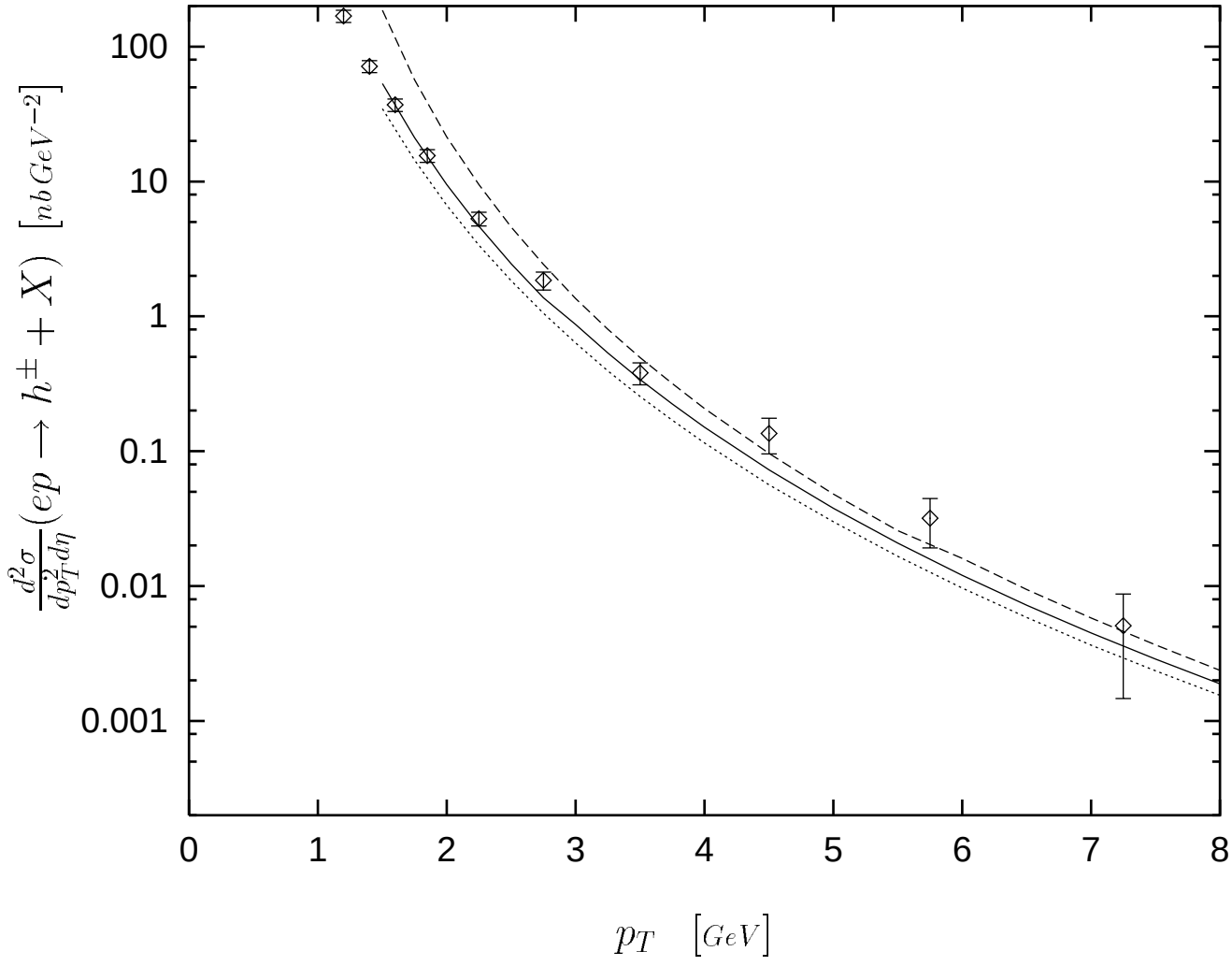
100
10
1
0.1
0.01
0.001
0
1
2
3
4
5
6
7
8
$\frac{d^2\sigma}{dp_T^2 d\eta}(ep \to h^{\pm} + X) \quad [nb\,GeV^{-2}]$
$p_T \quad [GeV]$

Fig. 8

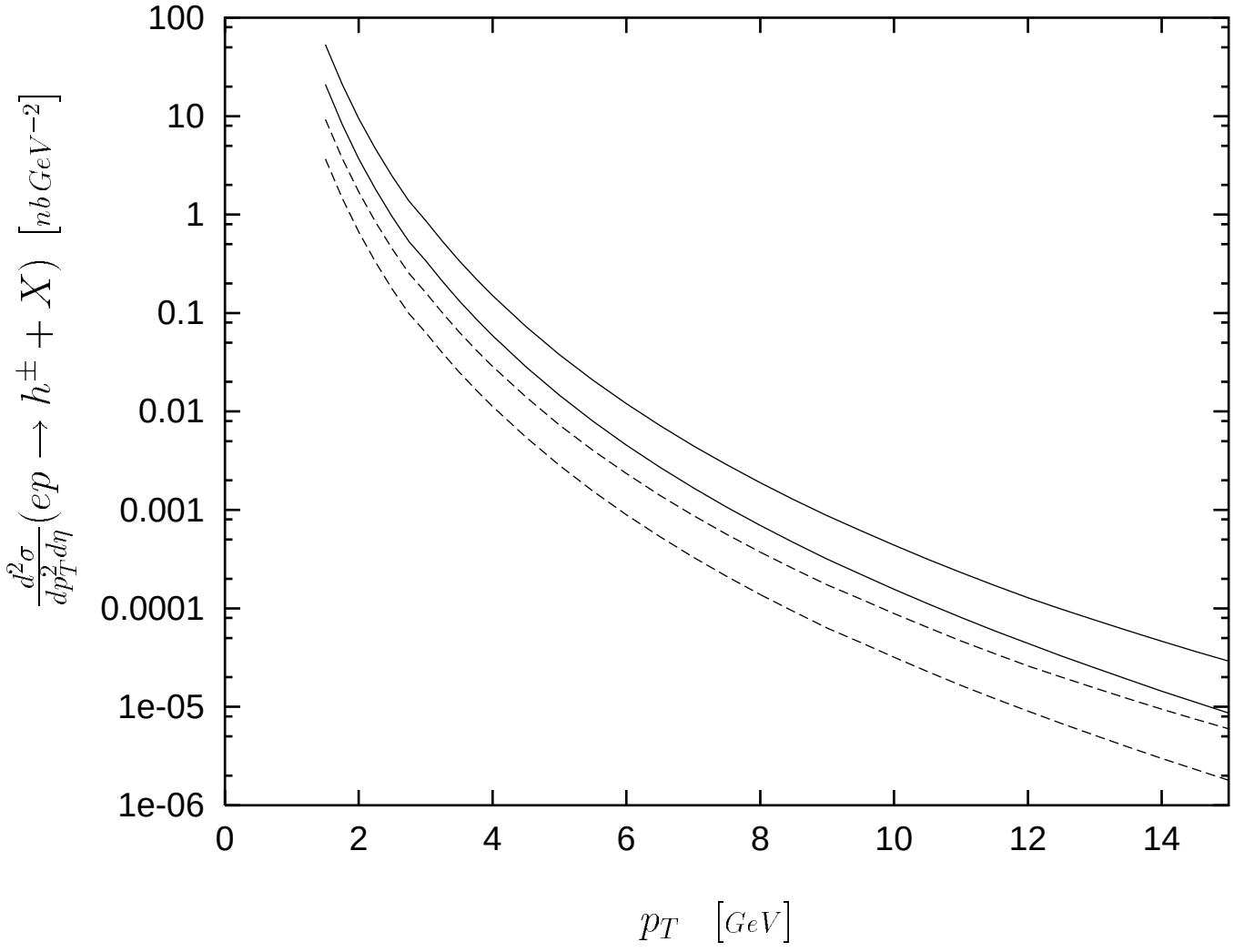
100
10
1
0.1
0.01
0.001
0.0001
1e-05
1e-06
0
2
4
6
8
10
12
14
$\frac{d^2\sigma}{dp_T^2 d\eta}(ep \to h^{\pm} + X)$ $\left[nb\,GeV^{-2}\right]$
p_T $\left[GeV\right]$

Fig. 9

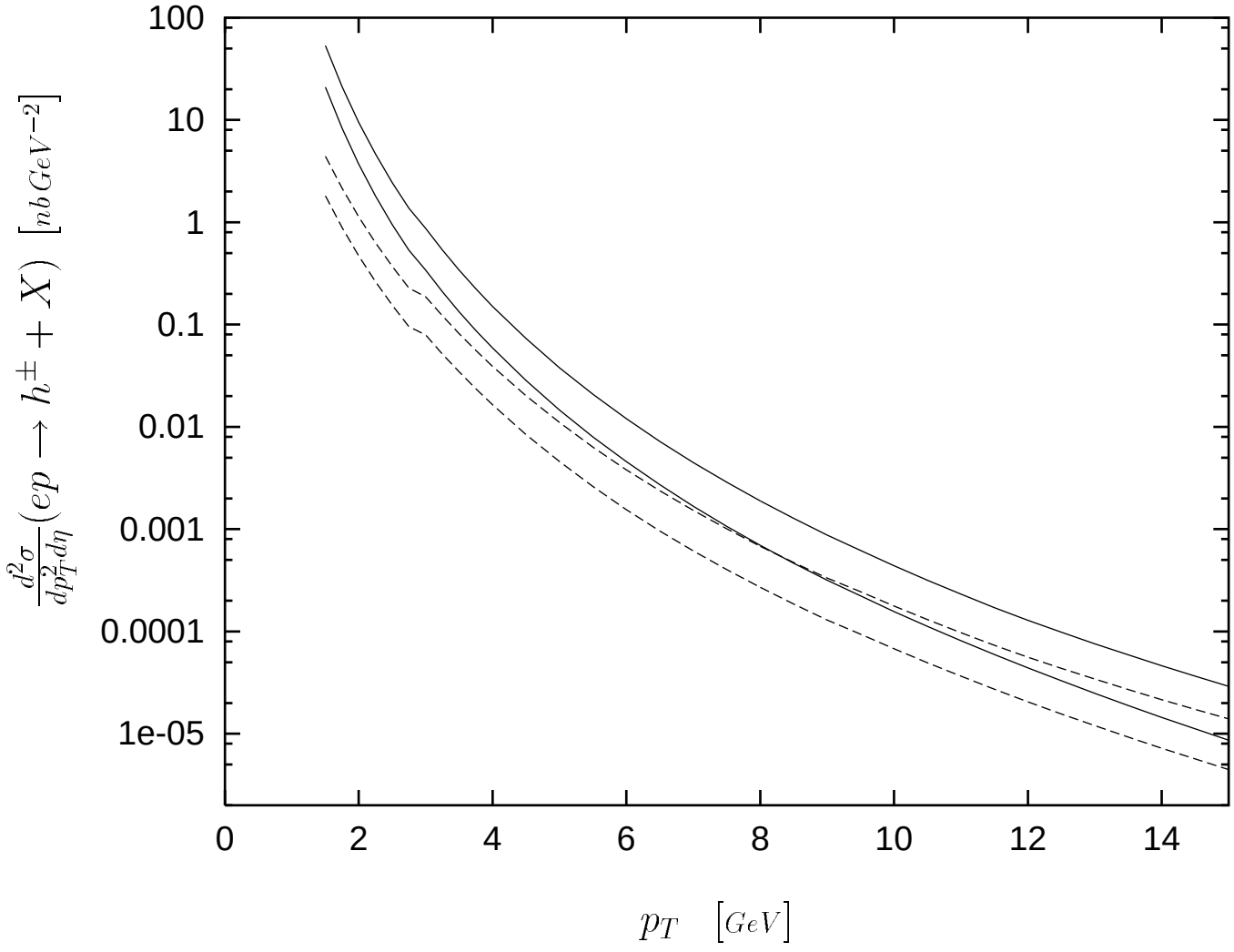
100
10
1
0.1
0.01
0.001
0.0001
1e-05
0
2
4
6
8
10
12
14
$\frac{d^2\sigma}{dp_T^2 d\eta}(ep \to h^{\pm} + X)$ $[nb\,GeV^{-2}]$
p_T $[GeV]$

Fig. 10